Two phytoplasmas elicit different responses in the insect vector *Euscelidius variegatus* Kirschbaum

Running title: Vector-borne plant pathogens modulate insect immunity

Luciana Galetto[a]#, Simona Abbà[a], Marika Rossi[a], Marta Vallino[a], Massimo Pesando[a], Nathalie Arricau-Bouvery[b], Marie-Pierre Dubrana[b], Walter Chitarra[a,c], Mattia Pegoraro[a], Domenico Bosco[a,d], Cristina Marzachì[a]

[a]Istituto per la Protezione Sostenibile delle Piante, CNR, National Research Council of Italy, IPSP-CNR, Torino, Italy

[b]INRA, Univ. Bordeaux, UMR Biologie du Fruit et Pathologie, UMR 1332, Villenave d'Ornon Cedex, France

[c]Centro di Ricerca per la Viticoltura e l'Enologia, CREA, Council for Agricultural Research and Economics, CREA-VE, Conegliano (TV), Italy

[d] Dipartimento di Scienze Agrarie, Forestali ed Alimentari DISAFA, Università degli Studi di Torino, Grugliasco (TO), Italy

#Corresponding author: Luciana Galetto, luciana.galetto@ipsp.cnr.it

ABSTRACT

Phytoplasmas are plant pathogenic bacteria transmitted by hemipteran insects. The leafhopper *Euscelidius variegatus* is a natural vector of chrysanthemum yellows phytoplasma (CYp) and a laboratory vector of Flavescence dorée phytoplasma (FDp). The two phytoplasmas induce different effects on this species: CYp slightly improves, while FDp negatively affects insect fitness. To investigate the molecular bases of these different responses, RNA-seq analysis of *E. variegatus* infected with either CYp or FDp was performed. The sequencing provided the first *de novo* transcriptome assembly for a phytoplasma vector, and a starting point for further analyses on differentially regulated genes, mainly related to immune system and energy metabolism. Insect phenoloxidase activity, immunocompetence, and body pigmentation were measured to investigate the immune response, while respiration and movement rates were quantified to confirm the effects on energy metabolism. The activation of insect immune response upon FDp infection, which is not naturally transmitted by *E. variegatus*, confirmed that this bacterium is mostly perceived as a potential pathogen. Conversely, the acquisition of CYp, which is naturally transmitted by *E. variegatus*, seems to increase the insect fitness by inducing a prompt response to stress. This long-term relationship is likely to improve survival and dispersal of the infected insect, thus enhancing the opportunity of phytoplasma transmission.

INTRODUCTION

Phytoplasmas are wall-less plant pathogenic bacteria of the class Mollicutes~~,~~ that cause yield losses in many crops worldwide. They colonize plant phloem tissues and are transmitted by phloem-feeding hemipterans (1). In insects, ingested phytoplasmas cross the gut, multiply in the haemocoel and invade salivary glands, before being transmitted during feeding on a new plant (2). Currently, genomes of four phytoplasmas are fully sequenced and annotated and few others are available as drafts (1). Phytoplasmas have small genomes (~750 kb) due to a genome reduction that resulted in the loss of important metabolic pathways: as a consequence, these intracellular bacteria depend on

47 their hosts for many essential metabolites (3). Due to these strict interactions with hosts and to the
48 difficulty of their axenic cultivation, phytoplasmas need to be studied directly in their hosts. Little is
49 known about pathogenicity mechanism, even if some pathogen-secreted virulence factors have been
50 identified, mainly in strains of '*Candidatus* Phytoplasma asteris' (2). Studies on this species suggest
51 that phytoplasmas are able to modulate their gene expression during host switching between plant
52 and insect (4, 5).
53 Flavescence dorée (FD) is an important grapevine disease caused by a 16SrV phytoplasma, mainly
54 transmitted~~,~~ under field conditions~~,~~ by the hemipteran cicadellid *Scaphoideus titanus*. FD
55 phytoplasma (FDp) is a plant quarantine pathogen in the European Union and represents one of the
56 major threats to southern European viticulture. *Vitis vinifera* and *S. titanus* do not represent ideal
57 experimental organisms for laboratory tests: grapevine is a perennial woody plant and the
58 leafhopper is a monovoltine species. Thus, a laboratory model has been established to manage FDp
59 infection cycle with the herbaceous *Vicia faba* as plant and the polivoltine leafhopper *Euscelidius*
60 *variegatus* as vector (6).
61 Chrysanthemum yellows phytoplasma (CYp), 16SrI-B '*Ca*. P. asteris', is associated with a disease
62 of ornamental plants in north-western Italy, where *E. variegatus* is one of the most important
63 natural vectors (7). Like FDp, CYp infections can be obtained under controlled conditions with
64 *Chrysanthemum carinatum* as host plant and *E. variegatus* as vector. The two phytoplasmas have
65 opposite effects on the vector fitness: FDp significantly reduces insect longevity and fecundity (8),
66 meanwhile CYp induces a slight fitness increase (9). CYp shows greater ability than FDp to
67 colonise the salivary glands of the vector and therefore it is more efficiently transmitted by *E.*
68 *variegatus* (7). So far, physical maps of FDp and CYp genomes, drafts of their genome sequences
69 and an FDp transcriptome analysis (10) are available. By contrast, neither the genome nor the
70 transcriptome of *E. variegatus* is available. Few proteins of the insect have been identified, such as
71 *in vitro* interacting partners of CYp antigenic membrane protein (Amp) (11), which is necessary for
72 CYp acquisition by insect vectors (12). The specificity of FDp transmission is presumably mediated

by variable membrane protein A (VmpA), a phytoplasma protein that is supposed to interact with insect tissues and shows high sequence variability in different strains transmitted by different vector species (13).

In a few studies the plant response to phytoplasma infection was addressed with NGS transcriptomic approaches (1), but to our knowledge this technique has never been used to investigate either the transcriptomic profile of an insect vector infected by these pathogens or the alterations induced by different phytoplasmas in the same host. Here we investigated the effects of two genetically different phytoplasmas on the same insect vector, providing: i) *de novo* assembly of *E. variegatus* transcriptome, ii) differential expression analysis of *E. variegatus* transcripts under infection with CY or FD phytoplasmas iii) validation of the differential expression profiles and iv) biological experiments to support the transcript profiling results.

RESULTS

RNAseq and differential gene expression. Diagnostic RT-qPCR assays confirmed the presence of CY and FD phytoplasmas in *E. variegatus* samples (Eva_CY and Eva_FD). The phytoplasma populations, expressed as mean phytoplasma 16S/insect18S ratio, were 4.67E-03 (SEM ± 9.84 E-04) and 2.08 E-04 (SEM ± 6.54 E-05) for insects infected with CYp and FDp, respectively.

Analyses of the cDNA libraries obtained from Eva_CY and Eva_FD resulted in a combined *de novo* assembly comprising around 135,000 transcripts, with an average GC content of 40%, a median contig length of 433 bp, and an average contig length of 833 bp. Due to the lack of genomic sequence information of *E. variegatus*, the functional annotation of transcripts was conducted using blastx against the NCBI non-redundant (nr) database. The Blast2GO platform was then used to assign the Gene Ontology (GO) terms to the predicted proteins with known function. The results of the *de novo* assembly and the following transcript annotations are summarized in Table S1. The species distributions of the best blastx matches for each sequence are shown in Table S2.

Transcriptome profiles of *E. variegatus* infected by the beneficial CY or the pathogenic FD phytoplasmas were compared to elucidate the differential vector responses.

Differential expression analysis revealed that 84 transcripts were up-regulated and 13 down-regulated in Eva_CY in comparison with Eva_FD (Tables 1 and 2, S3 and S4). The up-regulated genes could be classified in few main functional categories: immune response (11 transcripts), movement and energy metabolism (34 transcripts), proteases (9 transcripts), extracellular matrix (20 transcripts), nucleic acid binding (6 transcripts), and detoxification (4 transcripts). Down-regulated genes could be ascribed to immune response (10 transcripts), movement and energy metabolism (1 transcript), proteases (1 transcript), and detoxification (1 transcript) functional categories. Some of these putative metabolic functions were further investigated to explore the phenotypes correlated with the altered gene regulation.

Cellular and humoral immunity in response to phytoplasma infections. To investigate the effects of the phytoplasma presence on immune response, gene expression analysis of selected transcripts, enzymatic activity and biological assays were performed (Fig. 1A; Tables S5, S6, S7). Healthy controls (Eva_H), not exposed to phytoplasmas and PCR negative, were included in the following experiments to highlight the mechanisms underpinning the differential effects on *E. variegatus* immune response upon infection with the two phytoplasma species. Gender was taken into account, but whenever no sex-related differences were recorded within the same category data were pooled. RT-qPCR validation was run on 42 samples (each made up of five pooled insects), phenoloxidase activity was measured for 36 samples (each made up of haemolymph collected from five insects), pigmentation and immunocompetence assays were tested on 170 and 46 specimens, respectively.

Gene expression. Kazal-type 1 serine protease inhibitor and phenoloxidase genes were selected from the RNAseq results and literature search (14), respectively, and analysed by RT-qPCR in CYp-, FDp-infected and healthy insects (Eva_H, _CY, _FD). Similar levels of phenoloxidase transcripts were recorded in the insects, regardless of the sex and the infection status (Fig. 2A),

whereas Kazal-type 1 transcripts were significantly more abundant in Eva_FD males compared to Eva_CY ones (P=0.022) (Fig. 2B). Transcripts of the same gene were significantly more abundant in healthy females compared to healthy (P=0.002) and CYp-infected males (P=0.023) (Table S5). Up-regulation of Kazal-type 1 serine protease inhibitor in Eva_FD confirmed the differential expression obtained by RNAseq analysis (Table 2).

Enzymatic activity. Phenoloxidase (PO) and Pro-PO activities associated with haemocytes and the plasma fraction of haemolymph were quantified. The specific inhibitor phenylthiourea inhibited PO and ProPO activities in all assays with the exception of PO in haemocytes (data not further analyzed). The PO activities of the plasma fractions were similar irrespective of sex and infection status (Table S6). The plasma ProPO activities were significantly lower in males than in females, irrespective of the infection status (P<0.001, P<0.001 and P=0.018, for H, CY and FD, respectively); this activity was higher in FDp- compared to CYp-infected insects (two-fold increase), although the difference was significant only for males (P=0.046) (Fig. 2C). ProPO activities were similar in haemocytes from females and males of each infection status, whereas the enzymatic activity of Eva_FD was double than that of Eva_CY (P=0.017) (Fig. 2D). Steeper slopes of the linear phases of Eva_FD assays further confirmed faster enzymatic reactions in FDp-infected insects (Table S6).

Pigmentation assay. Since PO activity may be correlated to cuticular colour (15), pigmentation of bodies (dorsal side) and forewings of healthy and phytoplasma-infected *E. variegatus* was further explored. Pigmentation was expressed as grey intensity: 0 for black to 255 for white (Fig. 2E). Considering the three experimental conditions (Eva_H, _CY, _FD), males always showed significantly darker bodies and wings than females (P=0.005 for healthy bodies and P<0.001 for all other comparison) (Table S7). Wing pigmentation did not show any significant variation in the presence of phytoplasmas, while bodies of FDp-infected female and male insects were significantly darker than healthy and CYp-infected ones (female: P<0.001 for both comparison; male: P<0.001 and P=0.003 for H vs. FD and CY vs. FD, respectively) (Fig. 2E).

150 *Immunocompetence assay.* To determine whether the phytoplasma presence could influence insect
151 immune response, nylon threads were implanted in insect abdomens to measure melanization as
152 well as the number of haemocytes adhered to the threads (Fig. 2F, Table S7). There was no
153 influence of sex on melanization index (MI) and number of cells adherent to the nylon threads,
154 irrespective of the infection status, but there was a significant difference of MIs of nylon threads
155 implanted in CYp-infected *E. variegatus* compared to those implanted in healthy insects (Fig. 2F,
156 bars). Up to five times more haemocytes adhered to nylon threads implanted into CYp-infected *E.*
157 *variegatus* compared to those implanted into H and FDp-infected insects, and this difference was
158 significant in both cases ($P<0.001$) (Fig. 2F, dots).
159 **Movement and energy metabolism.** Genes involved in muscle contraction and synthesis of
160 intermediate metabolites for energy production were selected among those differentially regulated
161 according to the RNAseq results and literature search (16) (Fig. 1B; Table S5). To investigate the
162 effects of phytoplasma infection on insect mobility and respiration rate, several parameters were
163 measured (Fig. 3F, G, H), (Table S8). Healthy controls (Eva_H) were included in the following
164 experiments to better describe the metabolic response of *E. variegatus* challenged by the two
165 phytoplasmas, and whenever no sex-related differences were recorded within the same category
166 data were pooled. RT-qPCR validation was run on 42 samples (each made up of five pooled
167 insects), movement assay was tested on 138 specimens and CO_2 production was measured in 24
168 insect groups (each made up of three specimens).
169 *Gene expression.* Myosin light chain, tropomyosin, arginine kinase and maltase were analysed by
170 RT-qPCR in insects of the three experimental conditions (Eva_H, _CY, _FD). The four analysed
171 transcripts were significantly more abundant in males than in females, regardless of the infection
172 status, with the exception of tropomyosin and arginine kinase in healthy insects (Fig 3A-D, Table
173 S5). In general, CYp-infected males showed higher transcript levels compared to healthy and FDp-
174 infected males. These differences were significant only for tropomyosin, with about three times
175 more transcripts in CYp-infected vs. healthy males ($P=0.018$) and for arginine kinase, with about

176 twice more transcripts in CYp-infected males vs. healthy and FDp-infected ones (P<0.001 for both
177 comparison). Arginine kinase transcripts were also significantly more abundant in CYp-infected
178 females compared with FDp-infected ones (P=0.024) (Fig. 3C). Up-regulation of arginine kinase
179 and maltase in Eva_CY confirmed the differential expression results of the RNAseq analysis (Table
180 1).

181 *Protein expression.* To further characterize the differential expression of proteins involved in
182 movement, Western blot analysis was performed on healthy and phytoplasma-infected insects with
183 anti-tropomyosin commercial antisera (Figs. 3I and S1). Tropomyosin was more expressed in males
184 than in females, regardless of the infection status, therefore confirming the transcriptional analyses.
185 Nevertheless, there were no evident differences in protein expression levels among Eva_H, _CY
186 and _FD categories.

187 *Movement and respiration functional assays.* Movement parameters (permanence time in a two
188 circle arena and numbers of jumps) showed neither significant variation between males and
189 females, nor among the three experimental conditions, although a trend of a faster movement was
190 observed for CYp-infected males in comparison with healthy and FDp-infected ones (Fig. 3E, bars;
191 Table S8). Consistently, measurements with the gas analyzer showed that Eva_CY produced a
192 significantly higher amount of CO_2 than Eva_H and _FD, irrespective of sex (P=0.002 and P=0.027
193 for H vs. CY and CY vs. FD, respectively) (Fig. 3E, dots; Table S8).

194 **Protease regulation.** Cathepsin L was selected to investigate the effect of phytoplasma infection on
195 protease regulation. This protein is the major component of the gut digestive enzymes in many
196 invertebrates (17) and, among other functions, is involved in controlling symbiont populations (18).
197 Healthy controls (Eva_H) were included in the following experiments, to dissect the effects of the
198 different phytoplasmas on *E. variegatus* protease regulation.

199 *Gene expression.* The expression profile of four isoforms (namely 92i3, 92i4, 92i6 and 473) of
200 cathepsin L was analysed by RT-qPCR in insects of the three experimental conditions (Eva_H,
201 _CY, _FD). Isoform 473 was the most strongly up-regulated in Eva_CY within the protease

category (Table 1), whereas isoforms 92i3, 92i4, 92i6 were selected since, among all *E. variegatus* transcripts annotated as "cathepsin L", they showed the highest identity with the immunogenic peptide recognized by the commercial anti-cathepsin L antibody used for the Western blot. Significant differences between female and male insects were present for isoform 473, irrespective of the infection status (up-regulated in females, $P=0.007$, $P<0.001$ and $P<0.001$, for Eva_H, CY and FD, respectively) and for isoforms 92i3 and 92i6 specifically for FDp-infected *E. variegatus* (up-regulated in males, $P=0.043$ and $P=0.017$ for 92i3 and 92i6, respectively) (Fig. 4A-D and Table S5). Transcripts of isoforms 92i3 and 92i4 were significantly up-regulated in CYp-infected females vs. FDp-infected ones ($P=0.012$ and $P=0.023$ for 92i3 and 92i4, respectively) (Fig. 4A and B). Those of isoform 473 were twice more abundant in CYp-infected females vs. healthy and FDp-infected ones, and these differences were significant ($P=0.003$ and $P=0.012$, for H vs. CY and CY vs. FD, respectively) (Fig. 4D). Up-regulation of cathepsin L_473 in Eva_CY compared to Eva_FD confirmed the results of the RNAseq analysis (Table 1).

Putative protein characterization. The predicted amino acid sequences of the four cathepsin L isoforms were analysed (Fig. 4E and F). All four isoforms showed putative signal peptide from aa 1-16, a pro-region containing the propeptide inhibitor domain and a predicted mature protein including the cysteine protease domain. Putative glycosilation sites were predicted on different isoforms: 2 nitrogen-linked and 5 oxygen-linked. Isoform 92i6 showed a unique putative N-linked site at position 37 and the isoform 473 missed an O-linked site at position 125. Isoforms 92i4 and 92i6 showed highly similar pre-proteins and identical mature forms, whereas isoforms 473 and 92i3 were the most diverse ones (Fig. 4F). The immunogenic peptide, recognized by the commercial antibody used for Western blot, was more similar to isoform 473 than the other ones (Fig. 4F).

Protein expression. To further characterize the effect of phytoplasma infection on the expression of cathepsin L protein, Western blot was performed on healthy and phytoplasma-infected insects with anti-cathepsin L commercial antisera (Figs. 4G and S1). The antibody was raised to detect both the pre-protein and the mature form, as it reacts against the immunogenic peptide indicated in Fig. 4E.

Indeed, the Western blots with anti-cathepsin L antibody (Fig. 4G) showed a complex pattern: two faint bands with high MW (around 37-35 kDa) possibly corresponding to pre-proteins, two intense bands with low MW (around 27-25 kDa) possibly corresponding to the mature forms. Similar band patterns were observed from total proteins of *E. variegatus* females, irrespective of the infection status. A similar profile, although less intense, was also evident for healthy males. Surprisingly, almost no signal from the lowest MW bands (25 kDa) was detected from phytoplasma-infected males.

DISCUSSION

Relationships between phytoplasmas and their vectors may be pathogenic, neutral or mutualistic (9). CYp and FDp establish different types of relationships with their vector *E. variegatus*: the former slightly improves vector fitness, the latter is pathogenic. The transcriptional landscape of *E. variegatus* infected with the two different phytoplasma species was analysed focusing on long lasting modifications occurring in insects during the response to chronic phytoplasma infection, thus avoiding any possible differences related to CYp and FDp multiplication dynamics during early stages of infection. Sex-specific effects were recorded for several of the tested parameters, as already described for immune response (19, 20) as well as insect movement and dispersal (21). Among insects of the *Cicadellidae* family, few *de novo* transcriptome assemblies are available: some were obtained from specific insect tissues, namely salivary glands of *Nephotettix cincticeps* (22) and *Empoasca fabae* (23) and intestinal tract of *Empoasca vitis* (24), others from whole bodies, such as those of *Graminella nigrifrons* (25), *Homalodisca vitripennis* (26) and *Zyginidia pullula* (27). Interestingly, the transcriptomic response of *G. nigrifrons* vector to different plant virus~~es~~ infections reveals that the expression of cytoskeleton and immunity genes increase in the presence of the persistent propagative rhabdovirus Maize fine streak virus (28).

Phytoplasma infection modulates insect immune response. Molecular and biological analyses indicate that a different modulation of *E. variegatus* immune response occurred following FDp infection compared to CYp infection.

The altered regulation of the immune system was revealed by RNAseq analysis during infection with both phytoplasmas. Among these, transcripts of the Kazal type 1 serine protease inhibitor were more abundant in FDp-infected insects compared to Eva_CY. Similar serine protease inhibitors have antibacterial activity against bacteria (29) as well as antifungal activity against both plant-pathogenic and entomopathogenic fungi, as inhibitors of microbial serine proteases (30). Serpin was the most strongly up-regulated transcript in CYp-infected insects, whereas the snake-like serine protease was among the most strongly down-regulated ones. Clip serine proteases, such as the snake-like ones, are involved in the activation of the ProPO proteolytic cascade in invertebrate immune systems (31, 32), while serpins from different arthropod species inhibit clip domain serine proteases by blocking the activation of ProPO melanization pathway (33, 34). The prophenoloxidase (ProPO) cascade is involved in melanization and encapsulation processes and provides arthropod immunity against bacteria, fungi, protozoan and parasites (34). The opposite regulation of these two transcripts correlates with the lower prophenoloxidase activity and with the less intense cuticular pigmentation observed in CYp-infected compared to FDp-infected insects. Cuticular color is related to immune response in insects (15), and the darker body pigmentation of FDp-infected *E. variegatus* suggests stimulation of melanization pathway due to a stronger activation of the immune response. The presence of FDp is perceived by the insect as a stress status and therefore it elicits an intense production of melanin. Indeed, prophenoloxidase activities of both plasma and haemocyte lysates were more intense in Eva_FD compared to _CY and _H. On the other hand, the infection with the two phytoplasmas had neither effect on naturally activated phenoloxidase (PO) activity, a good estimate of invertebrate immunocompetence (35), nor on the abundance of the corresponding transcripts. This could be due to the fact that the analyses were performed at late, chronic stages of phytoplasma infection, when colonization of the insect body

278 was complete (12). A burst of activated phenoloxidase is, in fact, expected at the onset of the
279 infectious event, as a defence reaction to the immunological challenge (35), as reported for
280 *Micrococcus luteus* infection of the leafhopper *Circulifer haematoceps* (36). Surprisingly, when
281 insects are challenged by an additional stress (wounding through nylon thread), the scenario
282 changes. In the immunocompetence assay, insertion of a nylon thread in the insect body mimics a
283 parasite invader and induces encapsulation. The response of FDp-infected insects is similar to that
284 of the healthy ones. On the contrary, CYp-infected insects showed higher MI and higher number of
285 haemocytes, indicating a better capacity of these insects to react to and isolate an invader. *E.*
286 *variegatus* is a natural vector of CYp and they share the same ecological niches: these factors could
287 have shaped the insect immune system to fight more promptly against incoming pathogenic
288 organisms.
289 The Kruppel-like factor, a zinc finger DNA-binding protein, is crucial to mediate white spot
290 syndrome virus (WSSV) infection in two different shrimp species (37), and two transcripts of this
291 gene were oppositely regulated in *E. variegatus* (more abundant in FDp-infected category),
292 suggesting a role for this protein in response to phytoplasma infection. On the other hand,
293 hexamerin transcripts were up-regulated upon CYp infection. Members of this protein family are
294 inducible effector proteins in insect immunity upon bacteria ingestion and have a putative role in
295 gut repair (38). Moreover, in the closely related mollicute-leafhopper association (*C.*
296 *haematoceps/Spiroplasma citri)* hexamerin is up-regulated following infection and is required for
297 vector survival after spiroplasma inoculation (36). Besides their role in energy metabolism (see
298 below), arthropod arginine kinases (AK) are also involved in stress response and innate immunity:
299 *Apis cerana* AK is induced by abiotic and biotic stresses (39), pacific oyster AK modulates
300 bactericidal immune response in haemolymph (40), and AK from shrimp *Fenneropenaeus chinensis*
301 has been hypothesized as putative receptor of the WSSV virus envelope protein (41). AK transcript
302 was up-regulated upon CYp infection, suggesting different potential roles for this protein during
303 infection with the two phytoplasmas.

304 Disulfide bonds are redox-controlled switches for pathogens invasion, and are involved in
305 regulating pathogen entry into the endocytic pathway of vertebrate (42) and some invertebrates (43,
306 44). Recently, a vesicle-mediated colonization of salivary glands has been suggested for CYp
307 infection of *E. variegatus* (12). Consistently, the protein disulfide-isomerase (five transcripts) and
308 the gamma-interferon inducible lysosomal thiol genes were up-regulated upon CYp infection,
309 supporting the involvement of the endocytic pathway in phytoplasma colonization of the host, as
310 described for *Leishmania*, *Listeria* and *Chlamydia* spp (42). Other bacterial pathogens have
311 developed strategies to interfere with host lipidation mechanisms (45). For example, *Salmonella*
312 *enterica* and *Legionella pneumophyla* exploit host prenylation to direct effector proteins to the
313 pathogen containing vacuole of the host cell (46). Interestingly, transcripts of the farnesyl –
314 geranylgeranyl transferases, the key enzyme of the prenylation pathway, were oppositely regulated
315 in *E. variegatus* (down-regulated in CYp-infected insects) suggesting different alteration of
316 vesicular trafficking upon infection with CYp and FDp. Phytoplasma may modulate the host
317 metabolism through active secretion of effector molecules and the diversity of the effector arsenals
318 among phytoplasmas (2, 47) may explain the opposite transcription profiles of this gene.
319 **Chrysanthemum yellows phytoplasma infection increases energy metabolism.** Molecular and
320 biological analyses indicate an activation of *E. variegatus* energy production metabolism and an
321 increased locomotion activity upon CYp infection. According with RNAseq results, movement and
322 energy production metabolism was the functional category with the highest number of gene
323 transcripts altered upon phytoplasma infection.
324 Titin, twitchin and protein unc-89 are members of the giant cytoskeletal kinase family that mediate
325 sensing and transduction of mechanical signals in the myofibril. These big proteins display elastic
326 conformational deformation and regulate muscle tissue in adaptation to external stimuli (48).
327 Several isoforms of these gene transcripts were up-regulated in CYp-infected *E. variegatus*. These
328 kinases participate in regulating protein turnover in muscle, and, in particular, unc-89 regulates

329 ubiquitin-mediated protein degradation, through recruitment of E3 ubiquitin ligases (48), which
330 indeed was also up-regulated upon CYp infection.
331 Two isoforms of PDZ and LIM domain protein 3 were up-regulated in CYp-infected insects.
332 PDZ/LIM genes encode a large group of proteins that play important and diverse biological roles,
333 but that functionally can all influence or be associated with the actin cytoskeleton (49). Ryanodine
334 receptor (RYR) is the main calcium release complex of the sarcoplasmic reticulum involved in the
335 excitation-contraction coupling of muscle cells (50), and the dihydropyridine receptor (DHPR) is
336 the plasma membrane L-type calcium channel involved in opening of the RYR by a calcium-
337 induced calcium release mechanism (51). Transcripts of these genes were inversely regulated (RYR
338 up-regulated and DHPR down-regulated) upon CYp infection, suggesting an altered Ca^{2+} regulation
339 in the cytosol of muscle cells in response to phytoplasmas. Indeed, transcripts of the calcium-
340 transporting ATPase sarcoplasmic/endoplasmic reticulum (SERCA) and of the sarcalumenin were
341 up-regulated in CYp-infected insects. The former is a pump involved in translocation of cytosolic
342 calcium into the sarcoplasmic reticulum to allow relaxation of muscle fibers (16), the latter is a
343 calcium-binding protein involved in fine regulation of cellular calcium storage (52). Moreover,
344 transcripts of the main proteins involved in contraction and cytoskeletal motion, tropomyosin,
345 troponin, myosin, actin and dynein (16) were all up-regulated upon CYp infection. The analysis of
346 tropomyosin confirmed the stronger expression in males than in females, as revealed by RT-qPCR
347 and Western blot, but no evident differences were detected among different infection categories (H,
348 CY, FD), possibly due to several isoforms derived from alternative splicing, a well-known
349 phenomenon for this gene (53). Increased insect movement has been observed in some pathogen-
350 vector associations, such as *Diaphorina citri* infected with '*Candidatus* Liberibacter asiaticus' (54)
351 and *Bombyx mori* with BmNPV (55). We tested the intriguing hypothesis that CY phytoplasma,
352 which is naturally transmitted by the insect host, can manipulate the vector movement to increase its
353 transmission, but the parameters recorded during the movement assays did not clearly support this
354 hypothesis. Despite that, muscle contraction is also involved in active insect respiration, so the

355 higher expression of the above-mentioned genes in CYp-infected insects could be related with an
356 increase of the respiration rate. This was indeed the case, as higher CO_2 levels were produced by
357 CYp-infected *E. variegatus* in the respiration assay compared to FDp-infected and healthy insects.
358 Additionally, the up-regulation of maltase, hydroxybutyrate dehydrogenase and arginine kinase
359 (AK) transcripts in CYp-infected *E. variegatus* indicates a stronger activation of the energy
360 production metabolism. Altogether these data point to an augmented movement in CYp-infected
361 insect, which may positively influence phytoplasma transmission.
362 **Phytoplasma infection alters protease regulation.** Cathepsins are proteases generally stored in
363 lysosomes, involved in several processes like development, apoptosis and immunity of arthropods
364 (17, 56). Upon CYp infection, transcripts of cathepsin L were up-regulated and those of cathepsin D
365 down-regulated, suggesting different roles of these enzymes in response to phytoplasma infection.
366 To confirm RNAseq analysis, four isoforms were chosen among all the *E. variegatus* "cathepsin L"
367 transcripts: 473, derived from differential expression analysis, and 92i3, 92i4, 92i6, showing the
368 highest identity with the immunogenic peptide recognized by the anti-cathepsin L antibody used in
369 Western blot. The up-regulation of cathepsin L was confirmed by RT-qPCR for three of the four
370 isoforms upon CYp infection in comparison with FDp. The same up-regulation was not present at
371 protein level. Molecular weights of cathepsin L mature proteins differed from the theoretical ones
372 and this may be explained by different glycosylation, one of the post translational-processes
373 occurring during cathepsin maturation (57). Indeed the anti-cathepsin L antibody detected proteins
374 of different sizes, and intriguingly the lowest ones were poorly present in healthy males and nearly
375 absent in phytoplasma-infected males. As transcripts of isoform 473 were significant up-regulated
376 in females, these lowest protein bands are presumably its mature forms. Indeed isoform 473 showed
377 one glycosilation site less than other isoforms and could migrate faster. The absence of mature form
378 of this isoform in infected males might indicate that phytoplasma presence could prevent cathepsin
379 L maturation. Expression of this gene is altered upon microbial infection, either in pathogenic
380 combinations, such as *Serratia marcescens* in the pea aphid *Acyrthosiphon pisum* (18), and in

symbiotic associations, such as *Burkholderia* symbionts ingested by the bean bug *Riportus pedestris* (58). Indeed, both in pathogenic and mutualistic associations, bacteria need to avoid lysosomal degradation to establish an intracellular association and this could be true also for CY and FD phytoplasmas.

In conclusion, transcriptomic and phenotypic results shed some light on the molecular mechanisms underlying the different effects of the two phytoplasmas on the insect vector *E. variegatus*. Our data show that *E. variegatus* perceives FD as a pathogen, since it activates an immune response. Lack of natural interactions between FD phytoplasma, mainly restricted to *Vitis* spp., and the laboratory vector *E. variegatus*, which does not feed on grapevine, may explain perception of this phytoplasma as non-self. On the other hand, the long-lasting interactions between CY phytoplasma and *E. variegatus* (that are sympatric) might have driven towards a mutualistic relationship.

The prompt and aggressive response to the menace of an external pathogen, mimicked by the nylon thread, may be due to an immune priming activated by CYp and together with the increased energy metabolism are likely to provide an ecological advantage to both the vector and the phytoplasma.

MATERIALS AND METHODS

Insect and phytoplasmas. *E. variegatus* isolate to-1 was collected in Piedmont (Italy) and reared on oat, *Avena sativa* (L.) (7). Chrysanthemum yellows phytoplasma (CYp) was isolated in Italy, and maintained by insect transmission on daisy, *Chrysanthemum carinatum* Schousboe (7). Flavescence dorée phytoplasma (FDp) was isolated in Italy, and maintained by insect transmission on broad bean, *Vicia faba* L. Daisies, broad beans and oats were all grown from seed in greenhouses (59). For each acquisition access period (AAP), the sanitary status of source plants was confirmed by symptom observation and PCR as detailed in (4).

Three experimental conditions were set up. Fifth instar healthy nymphs were separately fed on i) healthy daisies and broad beans (Eva_H), ii) CYp-infected daisies (Eva_CY) or iii) FDp-infected

broad beans (Eva_FD) for an AAP of 7 days and then transferred on oat for a 28-day latency period (LP). At 35 days post acquisition survived insects were sexed, analyzed for phytoplasma infection and used.

RNA extraction. Total RNA was extracted from 64 samples (each made of 5 insects), nearly 20 for each experimental condition (10 female and 10 male) using Direct-zol RNA Mini Prep Kit (Zymo Research). RNA was analyzed in a Nanodrop spectophotometer and in a Bioanalyzer 2100 Expert Agilent Technologies, to evaluate concentration, purity and quality of the samples.

Phytoplasma detection and quantification. Total RNA was treated with Turbo RNase-free DNase I (Applied Biosystems). For CYp and FDp diagnosis, cDNA was synthesized from total RNA (800 ng) using High Capacity cDNA reverse transcription kit (Applied Biosystems). Two µl of cDNA were used as template in qPCR with iTaq Universal Probes Supermix (Bio-Rad) and primers CYS2Fw/Rv and TaqMan CYS2Probe (4). The same primers and probe, targeting phytoplasma 16SrRNA, and primers MqFw/Rv with TaqMan MqProbe, targeting insect 18SrRNA (4) were used to quantify phytoplasma load. Four serial 100-fold dilutions of p-GemTEasy (Promega) plasmids, harboring portions of ribosomal genes from phytoplasma and insect, were included to calculate phytoplasma16S/insect18S ratio.

RNA-seq, differential gene expression and sequence analysis. Six micrograms of RNA extracted from insects fed on phytoplasma-infected plants (Eva_CY; Eva_FD) and showing similar phytoplasma amount were sent to Macrogen (South Korea) for cDNA libraries construction and sequencing, as detailed in (59). Each library was obtained from a pooled sample of 20 males and 20 females. To generate a comprehensive landscape of the *E. variegatus* transcriptome, the datasets generated by the cDNA libraries (two biological replicates for each condition) were pooled, trimmed by Trimmomatic v0.32 (60), quality checked by FastQC v0.9(61), *de novo* assembled using Trinity v2.0.6 (62) and clustered by cd-hit-est (63) with a sequence identity cut-off = 0.98. Each transcript was analyzed by blastx against the NCBI nr database with a cut-off Expected value of 1e-04. Only transcripts with arthropods as best top hits species were retained for further analysis.

433 Functional annotation for each of the selected transcripts was obtained by loading the corresponding
434 XML output files in Blast2GO and running the mapping and the annotation options with default
435 parameters to retrieve GO terms and assign reliable functions, respectively. In addition, sequences
436 were analyzed for orthology predictions with eggnog (64) with DIAMOND mapping mode. Open
437 reading frames (ORF) were predicted by TransDecoder (65) using "--single_best_orf" and "--
438 retain_pfam_hits" options, which allow to retain only the single best ORF for each transcript
439 according to the presence of a significant Pfam hit.
440 Reads were loaded to NCBI's Sequence Read Archive (SRA) database with the following accession
441 numbers: SRR5816888, SRR5816889, SRR5816890, SRR5816891.
442 For differentially expressed gene (DEG) identification, DESeq2 package (66) v. 1.14.1 was run on a
443 60 core and 256 GB RAM local machine, running Ubuntu server 12.04 LTS. DEG selection was
444 based on an adjusted p-value ≤ 0.01 and a log2FC (Fold Change) ≥ 0.5 for up-regulated genes and $\leq$
445 -0.5 for down-regulated genes.
446 SignalP 4.1 (67), Prosite (68) and GlycoEP (69) were used to predict putative signal peptide, active
447 and glycosylation sites on cathepsin L isoforms, respectively. KEGG pathway database was used
448 for Fig. 1B preparation (70).
449 **qPCR validation.**
450 Some genes were selected from the RNAseq results and literature search and analyzed by RT-qPCR
451 in CYp-, FDp-infected and healthy insects (Eva_H, _CY, _FD). Reverse transcriptase reactions
452 were performed on the RNA extracted from 42 samples (each made up of five pooled insects):
453 seven samples of males and seven of females for each of the three conditions. These samples
454 included those used for library construction as well as new ones. Complementary DNA was used as
455 template for qPCR with primers in Table S9 and iTaq Universal SYBR Green Supermix (Bio-Rad)
456 with an annealing/extension temperature of 60°C. Primers were checked to target unique isoform in
457 the whole *E. variegatus* transcriptome. Among the six putative reference genes tested, the insect
458 elongation factor-1α, glutathione S-transferase and heat shock protein 70-1 were selected as the

most stable under the three conditions (Eva_H, Eva_FD and Eva_CY) (Table S10) and used for qPCR gene expression analysis, according to (71). Normalized relative quantities for each condition were compared.

Phenoloxidase activity. The enzymatic activity of naturally activated phenoloxidase (PO) and proenzyme prophenoloxidase (ProPO) were measured in plasma and haemocyte lysate supernatant (HLS) as described (35, 36). About 5 haemolymph samples were tested for each sex and condition. The optical density (OD) at 490 nm was determined immediately, after 30 min and then every hour for 15 h using a Bio-Rad Microplate Spectrophotometer. One unit of activity was defined as a change of 0.001 OD490nm per minute in the linear phase of reaction. Specificity was tested using phenylthiourea (Sigma, 4 mg/ml) to inhibit enzyme activity.

Pigmentation assay. The pigmentation of forewing and body (dorsal side) devoid of appendices was calculated through image analysis for about 50 insects for each condition. Images were taken under a stereomicroscope with a D5000 Nikon controlled by Camera Control Pro 2 software and analysed with Fiji software (72). The outline of the object to be measured was marked by the freehand selection tool. Light conditions, camera and software setting were not changed throughout image acquisition of the whole set of samples. Nevertheless, measure of each object was normalized against a white area used as internal standard. Mean degree of grey intensity was expressed as a numerical reading ranging from 0 for black to 255 for white.

Immunocompetence assay. A nylon thread (length 2-4 mm, Ø 80 µm) was implanted in abdomen of CO_2 anaesthetized insects under a stereoscope. About 50 insects were treated for each condition. Insects were transferred to oat for 72 h, collected and dissected to recover the nylon thread in 900 µl 10% PBS. Following overnight fixation at 4°C (4% paraformaldehyde, 0.1% Triton X100 in 10% PBS), the threads were washed, DAPI stained and photographed under light and UV microscope. Three images were taken at different z axes, to ensure the best count of nuclei of cell adherent to the thread. Image analyses was performed with Fiji software (72), and Melanization Index (MI) was calculated as the ratio between the integrated density per surface unit of nylon portions inside and

485 outside the body of each insect. About 15 insects were analysed for each condition. Number of
486 adherent cells were calculated by summing the DAPI stained nuclei in the three pictures of each
487 thread.

488 **Western blots.** For each category, proteins were extracted from four samples (each made up of five
489 pooled insects), quantified by Bradford reagent (Bio-Rad), and load on 12% polyacrylamide gels
490 (12 µg/lane), together with pre-stained and unstained broad range standards (Bio-Rad) (11). Gels
491 were either stained with colloidal Coomassie or blotted on PVDF membrane. Membranes were
492 blocked for 1 h (3% BSA in TBS 0.1% Tween, BSA-TBST), incubated overnight at 4°C with
493 primary antibodies (ab50567 rat-developed anti-tropomyosin, and ab200738 rabbit-developed anti-
494 cathepsin L, Abcam plc) both diluted 1:1000 in BSA-TBST, washed, incubated 2 h with
495 corresponding horseradish peroxidase conjugated secondary antibodies (A4416 GAM-HRP, and
496 A0545 GAR-HRP, Sigma, respectively) both diluted 1:10000 in BSA-TBST, washed and
497 developed with West Pico SuperSignal chemiluminescent substrate (Pierce) in a VersaDoc 4000
498 MP (Bio-Rad). Each experiment was repeated three times.

499 **Movement and respiration assays.** To evaluate insect movement among the three conditions,
500 insects were anaesthetized for 30 sec and put one at a time in the middle of two concentric circles
501 (Ø 2 and 6 cm) drawn on a paper, covered with a glass cylinder (height 20 cm) and continuously
502 observed for 5 min. Time required to leave the two circles and numbers of jumps were recorded.
503 About 20 insects were tested for each sex and condition.

504 To evaluate insect respiration, CO_2 production was monitored within the standard "broad leaf
505 chamber" of a LCpro+ (ADC BioScientific) gas analyzer, as described for *Drosophila* (73). To
506 measure gas exchange, groups of three adults (same sex and same category) were put in a mini-cage
507 (1.5 ml tube, deprived of bottom and sealed with net). To allow better survival, 200 µl of feeding
508 solution (12) were put in the mini-cage cap and covered by a parafilm layer. For each sex and
509 category, 4 groups were analysed. Each mini-cage was left 30 min in the chamber before measure

(5 reading replicates). The CO_2 production, expressed by the analyzer in µmol/sec m^2, was transformed in µl/h per insect according with (73).

Statistical analyses. Depending on normal or not normal distribution of data, t-test or Mann-Whitney test were used for sex comparison, ANOVA or Kruskal-Wallis for category comparison (H vs. CY vs. FD) (Table S11). Tukey or Dunn post-hoc tests were used following ANOVA or Kruskal-Wallis, respectively. Whenever no sex-related differences were recorded within the same category, female and male data were pooled. SIGMAPLOT 11 (Systat Software) was used.

Contributions of authors

Design of experiments: LG SA CM MR MV DB; RNAseq, bioinformatic analysis and differential gene expression profiling: SA; RT-qPCR validation, statistical analysis and protein expression: LG; phenoloxidase enzymatic activity: LG CM MPes; pigmentation assay: MR MV SA; immunocompetence assay: CM NAB MPD; movement assay: SA MR MV MPes LG; respiration assay: LG WC; insect rearing and plant production: MPeg. LG SA MR MV CM wrote the paper and all authors reviewed the manuscript.

Conflict of interest

The authors declare that they have no conflicts of interest with the contents of this article.

ACKNOWLEDGMENTS

The Authors thank Brigitte Batailler for helping with immunocompetence assay, Francesco Pennacchio and Gennaro Di Prisco, University of Naples Federico II, for helpful discussion and suggestions.

This work was part of the 'FitoDigIt' Project funded by Fondazione Cassa di Risparmio di Torino, Torino (Italy), within the 'Richieste Ordinarie 2014' and 'Richieste Ordinarie 2015' calls. MR and MPeg were supported by a fellowship funded by the following grant-making foundations: Fondazione Cassa di Risparmio di Cuneo, Fondazione Cassa di Risparmio di Torino, and Fondazione Cassa di Risparmio di Asti in the framework of the INTEFLAVI project. The funders had no role in study design, data collection and interpretation, or the decision to submit the work for publication.

REFERENCES

1. Marcone C. 2014. Molecular biology and pathogenicity of phytoplasmas. Ann Appl Biol 165:199–221.

2. Maejima K, Oshima K, Namba S. 2014. Exploring the phytoplasmas, plant pathogenic bacteria. J Gen Plant Pathol 80:210–221.

3. Oshima K, Maejima K, Namba S. 2013. Genomic and evolutionary aspects of phytoplasmas. Front Microbiol 4:230.

4. Pacifico D, Galetto L, Rashidi M, Abbà S, Palmano S, Firrao G, Bosco D, Marzachì C. 2015. Decreasing global transcript levels over time suggest that phytoplasma cells enter stationary phase during plant and insect colonization. Appl Environ Microbiol 81:2591–2602.

5. Oshima K, Ishii Y, Kakizawa S, Sugawara K, Neriya Y, Himeno M, Minato N, Miura C, Shiraishi T, Yamaji Y, Namba S. 2011. Dramatic transcriptional changes in an intracellular parasite enable host switching between plant and insect. PLoS ONE 6:e23242.

6. Caudwell A, Kuszala C, Larrue J, Bachelier J. 1972. Transmission de la Flavescence dorée de la fève à la fève par des cicadelles des genres *Euscelis* et *Euscelidius*. Ann Phytopathol No. hors série:181–189.

7. Rashidi M, D'Amelio R, Galetto L, Marzachì C, Bosco D. 2014. Interactive transmission of two phytoplasmas by the vector insect. Ann Appl Biol 165:404–413.

8. Bressan A, Clair D, Sémétey O, Boudon-Padieu É. 2005. Effect of two strains of Flavescence dorée phytoplasma on the survival and fecundity of the experimental leafhopper vector *Euscelidius variegatus* Kirschbaum. J Invertebr Pathol 89:144–149.

9. Bosco D, Marzachì C. 2016. Insect transmission of phytoplasmas, p. 319–327. *In* Brown, JK (ed.), Vector-mediated transmission of plant pathogens. APS Press, St. Paul, Minnesota.

10. Abbà S, Galetto L, Carle P, Carrère S, Delledonne M, Foissac X, Palmano S, Veratti F, Marzachì C. 2014. RNA-Seq profile of flavescence dorée phytoplasma in grapevine. BMC Genomics 15:1088.

11. Galetto L, Bosco D, Balestrini R, Genre A, Fletcher J, Marzachì C. 2011. The major antigenic membrane protein of '*Candidatus* Phytoplasma asteris' selectively interacts with ATP synthase and actin of leafhopper vectors. PLoS ONE 6:e22571.

12. Rashidi M, Galetto L, Bosco D, Bulgarelli A, Vallino M, Veratti F, Marzachì C. 2015. Role of the major antigenic membrane protein in phytoplasma transmission by two insect vector species. BMC Microbiol 15:193.

13. Arricau-Bouvery N, Duret S, Dubrana M-P, Batailler B, Desqué D, Béven L, Danet J-L, Monticone M, Bosco D, Malembic-Maher S, Foissac X. 2018. Variable membrane protein A of flavescence dorée phytoplasma binds the midgut perimicrovillar membrane of *Euscelidius variegatus* and promotes adhesion to its epithelial cells. Appl Environ Microbiol AEM.02487-17.

14. Howell L, Sampson CJ, Xavier MJ, Bolukbasi E, Heck MMS, Williams MJ. 2012. A directed miniscreen for genes involved in the *Drosophila* anti-parasitoid immune response. Immunogenetics 64:155–161.

15. Armitage SAO, Siva-Jothy MT. 2005. Immune function responds to selection for cuticular colour in *Tenebrio molitor*. Heredity 94:650–656.

16. Morano I. 2013. Muscles and Motility, p. 461–478. *In* Galizia, CG, Lledo, P-M (eds.), Neurosciences - From Molecule to Behavior: a university textbook. Springer Berlin Heidelberg, Berlin, Heidelberg.

17. Waniek PJ, Pacheco Costa JE, Jansen AM, Costa J, Araújo CAC. 2012. Cathepsin L of *Triatoma brasiliensis* (Reduviidae, Triatominae): sequence characterization, expression pattern and zymography. J Insect Physiol 58:178–187.

18. Renoz F, Noël C, Errachid A, Foray V, Hance T. 2015. Infection dynamic of symbiotic bacteria in the pea aphid *Acyrthosiphon pisum* gut and host immune response at the early steps in the infection process. PLOS ONE 10:e0122099.

19. Rolff J. 2002. Bateman's principle and immunity. Proc R Soc B Biol Sci 269:867–872.

588 20. Sheridan LAD, Poulin R, Ward DF, Zuk M. 2000. Sex differences in parasitic infections among
589 arthropod hosts: is there a male bias? Oikos 88:327–334.

590 21. Blaauw BR, Jones VP, Nielsen AL. 2016. Utilizing immunomarking techniques to track *Halyomorpha*
591 *halys* (Hemiptera: Pentatomidae) movement and distribution within a peach orchard. PeerJ 4:e1997.

592 22. Matsumoto Y, Suetsugu Y, Nakamura M, Hattori M. 2014. Transcriptome analysis of the salivary
593 glands of *Nephotettix cincticeps* (Uhler). J Insect Physiol 71:170–176.

594 23. DeLay B, Mamidala P, Wijeratne A, Wijeratne S, Mittapalli O, Wang J, Lamp W. 2012. Transcriptome
595 analysis of the salivary glands of potato leafhopper, *Empoasca fabae*. J Insect Physiol 58:1626–1634.

596 24. Shao E, Lin G, Liu S, Ma X, Chen M, Lin L, Wu S, Sha L, Liu Z, Hu X, Guan X, Zhang L. 2017. Identification
597 of transcripts involved in digestion, detoxification and immune response from transcriptome of
598 *Empoasca vitis* (Hemiptera: Cicadellidae) nymphs. Genomics 109:58–66.

599 25. Chen Y, Cassone BJ, Bai X, Redinbaugh MG, Michel AP. 2012. Transcriptome of the plant virus vector
600 *Graminella nigrifrons*, and the molecular interactions of Maize fine streak rhabdovirus transmission.
601 PLoS ONE 7:e40613.

602 26. Nandety RS, Kamita SG, Hammock BD, Falk BW. 2013. Sequencing and de novo assembly of the
603 transcriptome of the glassy-winged sharpshooter (*Homalodisca vitripennis*). PLoS ONE 8:e81681.

604 27. Asgharian H, Chang PL, Mazzoglio PJ, Negri I. 2014. Wolbachia is not all about sex: male-feminizing
605 *Wolbachia* alters the leafhopper *Zyginidia pullula* transcriptome in a mainly sex-independent manner.
606 Front Microbiol 5:430.

607 28. Cassone BJ, Cisneros Carter FM, Michel AP, Stewart LR, Redinbaugh MG. 2014. Genetic insights into
608 *Graminella nigrifrons* competence for Maize fine streak virus infection and transmission. PLoS ONE
609 9:e113529.

29. Kumaresan V, Harikrishnan R, Arockiaraj J. 2015. A potential Kazal-type serine protease inhibitor involves in kinetics of protease inhibition and bacteriostatic activity. Fish Shellfish Immunol 42:430–438.

30. Kim BY, Lee KS, Zou FM, Wan H, Choi YS, Yoon HJ, Kwon HW, Je YH, Jin BR. 2013. Antimicrobial activity of a honeybee (*Apis cerana*) venom Kazal-type serine protease inhibitor. Toxicon 76:110–117.

31. Monwan W, Amparyup P, Tassanakajon A. 2017. A snake-like serine proteinase (Pm Snake) activates prophenoloxidase-activating system in black tiger shrimp *Penaeus monodon*. Dev Comp Immunol 67:229–238.

32. Barillas-Mury C. 2007. CLIP proteases and *Plasmodium* melanization in *Anopheles gambiae*. Trends Parasitol 23:297–299.

33. Liu Y, Hou F, He S, Qian Z, Wang X, Mao A, Sun C, Liu X. 2014. Identification, characterization and functional analysis of a serine protease inhibitor (Lvserpin) from the Pacific white shrimp, *Litopenaeus vannamei*. Dev Comp Immunol 43:35–46.

34. Dubovskiy I, Kryukova N, Glupov V, Ratcliffe N. 2016. Encapsulation and nodulation in insects. Invertebr Surviv J 13:229–246.

35. Cornet S, Biard C, Moret Y. 2009. Variation in immune defence among populations of *Gammarus pulex* (Crustacea: Amphipoda). Oecologia 159:257–269.

36. Eliautout R, Dubrana M-P, Vincent-Monégat C, Vallier A, Braquart-Varnier C, Poirié M, Saillard C, Heddi A, Arricau-Bouvery N. 2016. Immune response and survival of *Circulifer haematoceps* to *Spiroplasma citri* infection requires expression of the gene hexamerin. Dev Comp Immunol 54:7–19.

37. Huang P-H, Lu S-C, Yang S-H, Cai P-S, Lo C-F, Chang L-K. 2014. Regulation of the immediate-early genes of white spot syndrome virus by *Litopenaeus vannamei* kruppel-like factor (LvKLF). Dev Comp Immunol 46:364–372.

633 38. Castagnola A, Jurat-Fuentes JL. 2016. Intestinal regeneration as an insect resistance mechanism to
634 entomopathogenic bacteria. Curr Opin Insect Sci 15:104–110.

635 39. Chen X, Yao P, Chu X, Hao L, Guo X, Xu B. 2015. Isolation of arginine kinase from *Apis cerana cerana*
636 and its possible involvement in response to adverse stress. Cell Stress Chaperones 20:169–183.

637 40. Jiang S, Jia Z, Chen H, Wang L, Song L. 2016. The modulation of haemolymph arginine kinase on the
638 extracellular ATP induced bactericidal immune responses in the Pacific oyster *Crassostrea gigas*. Fish
639 Shellfish Immunol 54:282–293.

640 41. Ma C, Gao Q, Liang Y, Li C, Liu C, Huang J. 2016. Shrimp arginine kinase being a binding protein of
641 WSSV envelope protein VP31. Chin J Oceanol Limnol 34:1287–1296.

642 42. Sun J. 2012. Roles of cellular redox factors in pathogen and toxin entry in the endocytic pathways, p.
643 61–90. *In* Ceresa, B (ed.), Molecular regulation of endocytosis. InTech.

644 43. Kongton K, McCall K, Phongdara A. 2014. Identification of gamma-interferon-inducible lysosomal thiol
645 reductase (GILT) homologues in the fruit fly *Drosophila melanogaster*. Dev Comp Immunol 44:389–
646 396.

647 44. Ren C, Chen T, Jiang X, Luo X, Wang Y, Hu C. 2015. The first echinoderm gamma-interferon-inducible
648 lysosomal thiol reductase (GILT) identified from sea cucumber (*Stichopus monotuberculatus*). Fish
649 Shellfish Immunol 42:41–49.

650 45. Al-Quadan T, Price CT, London N, Schueler-Furman O, AbuKwaik Y. 2011. Anchoring of bacterial
651 effectors to host membranes through host-mediated lipidation by prenylation: a common paradigm.
652 Trends Microbiol 19:573–579.

653 46. Hicks SW, Galán JE. 2013. Exploitation of eukaryotic subcellular targeting mechanisms by bacterial
654 effectors. Nat Rev Microbiol 11:316–326.

47. Anabestani A, Izadpanah K, Abbà S, Galetto L, Ghorbani A, Palmano S, Siampour M, Veratti F, Marzachì C. 2017. Identification of putative effector genes and their transcripts in three strains related to '*Candidatus* Phytoplasma aurantifolia'. Microbiol Res 199:57–66.

48. Mayans O, Benian GM, Simkovic F, Rigden DJ. 2013. Mechanistic and functional diversity in the mechanosensory kinases of the titin-like family. Biochem Soc Trans 41:1066–1071.

49. Velthuis AJW, Bagowski CP. 2007. PDZ and LIM domain-encoding genes: molecular interactions and their role in development. Sci World J 7:1470–1492.

50. Rossi D, Sorrentino V. 2002. Molecular genetics of ryanodine receptors Ca^{2+}-release channels. Cell Calcium 32:307–319.

51. Takekura H, Franzini-Armstrong C. 2002. The structure of Ca^{2+} release units in arthropod body muscle indicates an indirect mechanism for excitation-contraction coupling. Biophys J 83:2742–2753.

52. Ji T, Yin L, Liu Z, Shen F, Shen J. 2014. High-throughput sequencing identification of genes involved with *Varroa destructor* resistance in the eastern honeybee, *Apis cerana*. Genet Mol Res 13:9086–9096.

53. Ayme-Southgate A, Feldman S, Fulmer D. 2015. Myofilament proteins in the synchronous flight muscles of *Manduca sexta* show both similarities and differences to *Drosophila melanogaster*. Insect Biochem Mol Biol 62:174–182.

54. Martini X, Hoffmann M, Coy MR, Stelinski LL, Pelz-Stelinski KS. 2015. Infection of an insect vector with a bacterial plant pathogen increases its propensity for dispersal. PLOS ONE 10:e0129373.

55. Wang G, Zhang J, Shen Y, Zheng Q, Feng M, Xiang X, Wu X. 2015. Transcriptome analysis of the brain of the silkworm *Bombyx mori* infected with Bombyx mori nucleopolyhedrovirus: a new insight into the molecular mechanism of enhanced locomotor activity induced by viral infection. J Invertebr Pathol 128:37–43.

678 56. Saikhedkar N, Summanwar A, Joshi R, Giri A. 2015. Cathepsins of lepidopteran insects: aspects and
679 prospects. Insect Biochem Mol Biol 64:51–59.

680 57. Katunuma N. 2010. Posttranslational processing and modification of cathepsins and cystatins. J Signal
681 Transduct 2010:1–8.

682 58. Futahashi R, Tanaka K, Tanahashi M, Nikoh N, Kikuchi Y, Lee BL, Fukatsu T. 2013. Gene expression in
683 gut symbiotic organ of stinkbug affected by extracellular bacterial symbiont. PLoS ONE 8:e64557.

684 59. Abbà S, Galetto L, Vallino M, Rossi M, Turina M, Sicard A, Marzachì C. 2017. Genome sequence,
685 prevalence and quantification of the first iflavirus identified in a phytoplasma insect vector. Arch Virol
686 162:799–809.

687 60. Bolger AM, Lohse M, Usadel B. 2014. Trimmomatic: a flexible trimmer for Illumina sequence data.
688 Bioinformatics 30:2114–2120.

689 61. FastQC. 2016. https://www.bioinformatics.babraham.ac.uk/projects/fastqc/.

690 62. Haas BJ, Papanicolaou A, Yassour M, Grabherr M, Blood PD, Bowden J, Couger MB, Eccles D, Li B,
691 Lieber M, MacManes MD, Ott M, Orvis J, Pochet N, Strozzi F, Weeks N, Westerman R, William T,
692 Dewey CN, Henschel R, LeDuc RD, Friedman N, Regev A. 2013. De novo transcript sequence
693 reconstruction from RNA-seq using the Trinity platform for reference generation and analysis. Nat
694 Protoc 8:1494–1512.

695 63. Li W, Godzik A. 2006. Cd-hit: a fast program for clustering and comparing large sets of protein or
696 nucleotide sequences. Bioinformatics 22:1658–1659.

697 64. Powell S, Szklarczyk D, Trachana K, Roth A, Kuhn M, Muller J, Arnold R, Rattei T, Letunic I, Doerks T,
698 Jensen LJ, von Mering C, Bork P. 2012. eggNOG v3.0: orthologous groups covering 1133 organisms at
699 41 different taxonomic ranges. Nucleic Acids Res 40:D284–D289.

700 65. Transdecoder. 2016. https://transdecoder.github.io/.

66. Love MI, Huber W, Anders S. 2014. Moderated estimation of fold change and dispersion for RNA-seq data with DESeq2. Genome Biol 15:550.

67. Petersen TN, Brunak S, von Heijne G, Nielsen H. 2011. SignalP 4.0: discriminating signal peptides from transmembrane regions. Nat Methods 8:785–786.

68. Sigrist CJA, de Castro E, Cerutti L, Cuche BA, Hulo N, Bridge A, Bougueleret L, Xenarios I. 2013. New and continuing developments at PROSITE. Nucleic Acids Res 41:D344–D347.

69. Chauhan JS, Rao A, Raghava GPS. 2013. In silico platform for prediction of N-, O- and C-glycosites in eukaryotic protein sequences. PLoS ONE 8:e67008.

70. Kanehisa M, Furumichi M, Tanabe M, Sato Y, Morishima K. 2017. KEGG: new perspectives on genomes, pathways, diseases and drugs. Nucleic Acids Res 45:D353–D361.

71. Vandesompele J, De Preter K, Pattyn F, Poppe B, Van Roy N, De Paepe A, Speleman F. 2002. Accurate normalization of real-time quantitative RT-PCR data by geometric averaging of multiple internal control genes. Genome Biol 3:research0034.1.

72. Schindelin J, Arganda-Carreras I, Frise E, Kaynig V, Longair M, Pietzsch T, Preibisch S, Rueden C, Saalfeld S, Schmid B, Tinevez J-Y, White DJ, Hartenstein V, Eliceiri K, Tomancak P, Cardona A. 2012. Fiji: an open-source platform for biological-image analysis. Nat Methods 9:676–682.

73. Cooper R, McLetchie D. 2004. Monitoring carbon dioxide production by *Drosophila* larvae. Drosoph Inf Serv 87:88–91.

720 **Table 1. Overview of *Euscelidius variegatus* transcripts** up-regulated during chrysanthemum yellows (CYp) infection, compared with insects
721 infected by Flavescence dorée (FDp) phytoplasmas. Transcripts were classified into functional categories according to the putative identification
722 assigned by a blastx search.

Contig accession*	FPKM (Average±SD)		Ln Fold change	P value	Sequence description
	Eva_CY	Eva_FD			
Immune response					
GFTU01010641.1	69.0 ±1.4	39.9±5.6	+0.802	2E-14	PREDICTED: serpin B3-like
GFTU01009442.1	63.5±3.1	39.9±2.4	+0.729	2E-23	hypothetical protein g.45731 (Protein Disulfide Isomerase (PDIa) family, redox active TRX domains)
GFTU01009443.1	34.9±1.4	22.0±1.8	+0.723	7E-22	PREDICTED: uncharacterized protein LOC109042410 isoform X4 (Protein Disulfide Isomerase (PDIa) family, redox active TRX domains)
GFTU01009445.1	35.4±1.5	22.4±1.8	+0.721	6E-22	PREDICTED: uncharacterized protein LOC106678838 isoform X8 (Protein Disulfide Isomerase (PDIa) family, redox active TRX domains)
GFTU01009444.1	59.5±3.0	37.8±1.9	+0.717	6E-24	hypothetical protein g.45731 (Protein Disulfide Isomerase (PDIa) family, redox active TRX domains)
GFTU01012880.1	111.7±6.6	80.8±5.5	+0.518	6E-07	PREDICTED: protein disulfide-isomerase A6
GFTU01010415.1	40.3±0.4	26.3±4.8	+0.592	4E-05	PREDICTED: gamma-interferon-inducible lysosomal thiol reductase-like
GFTU01003389.1	30.9±2.2	20.9±2.9	+0.559	5E-05	hypothetical protein g.13589 (Single domain von Willebrand factor type C)
GFTU01000362.1	1136.7±171.8	589.7±137.6	+0.556	8E-3	PREDICTED: hexamerin 4 isoform X1
GFTU01005409.1	3.9±0.5	2.6±0.5	+0.548	2E-03	chitinase
GFTU01006368.1	14.7±0.3	10.8±0.6	+0.512	2E-09	PREDICTED: E3 ubiquitin-protein ligase HUWE1 isoform X5
Movement and energy metabolism					
GFTU01004258.1	57.3±3.3	27.7±0.2	+1.082	1E-43	PREDICTED: troponin I-like isoform X2
GFTU01000669.1	44.4±4.2	27.0±0.7	+0.719	8E-10	PREDICTED: maltase A1-like
GFTU01001629.1	47.1±0.9	28.5±0.9	+0.791	2E-32	PREDICTED: twitchin isoform X25
GFTU01012455.1	47.2±0.9	28.6±0.9	+0.791	2E-32	PREDICTED: twitchin isoform X19
GFTU01012453.1	47.5±0.9	28.7±0.9	+0.790	2E-32	PREDICTED: twitchin isoform X23
GFTU01001631.1	47.0±0.9	28.4±0.9	+0.790	2E-32	PREDICTED: twitchin isoform X1
GFTU01001630.1	47.4±0.9	28.7±0.9	+0.790	2E-32	PREDICTED: twitchin isoform X1
GFTU01001638.1	47.3±0.9	28.6±0.9	+0.790	2E-32	PREDICTED: twitchin isoform X1
GFTU01001632.1	47.3±0.9	28.7±0.9	+0.789	2E-32	PREDICTED: twitchin isoform X1
GFTU01001635.1	47.2±0.9	28.6±0.9	+0.789	2E-32	PREDICTED: twitchin isoform X1
GFTU01001634.1	47.7±0.9	28.9±0.9	+0.789	2E-32	PREDICTED: twitchin isoform X23
GFTU01001636.1	47.5±0.9	28.8±0.9	+0.789	2E-32	PREDICTED: twitchin isoform X25
GFTU01001637.1	47.3±1.0	28.7±0.9	+0.789	2E-32	PREDICTED: twitchin isoform X25
GFTU01001633.1	47.3±0.9	28.6±0.9	+0.789	2E-32	PREDICTED: twitchin isoform X24
GFTU01012458.1	54.6±0.3	34.6±0.3	+0.723	1E-26	PREDICTED: twitchin isoform X16
GFTU01012456.1	46.6±3.3	32.8±1.2	+0.567	2E-11	PREDICTED: twitchin isoform X13
GFTU01001910.1	1319.6±93.2	893.8±69.3	+0.633	3E-21	PREDICTED: arginine kinase
GFTU01009195.1	633.2±64.8	428.9±54.4	+0.618	2E-13	PREDICTED: myosin light chain alkali
GFTU01001677.1	1054.6±59.2	786.0±22.8	+0.506	6E-18	PREDICTED: myosin heavy chain, muscle isoform X30
GFTU01002981.1	76.1±1.5	51.4±0.3	+0.633	1E-17	PREDICTED: PDZ and LIM domain protein 3 isoform X3
GFTU01000140.1	79.3±1.4	53.6±0.7	+0.629	3E-17	PREDICTED: PDZ and LIM domain protein 3 isoform X4
GFTU01012488.1	35.2±1.0	24.1±0.1	+0.609	5E-16	PREDICTED: sarcalumenin isoform X2
GFTU01006510.1	1983.5±71.2	1262.8±211.9	+0.598	1E-4	actin muscle

GFTU01009078.1	9.6±0.0	6.5±0.6	+0.601	2E-07	PREDICTED: muscle M-line assembly protein unc-89 isoform X1
GFTU01012457.1	40.3±2.3	27.9±0.5	+0.595	2E-14	PREDICTED: muscle M-line assembly protein unc-89-like
GFTU01012454.1	37.0±2.0	25.8±0.8	+0.588	2E-13	PREDICTED: muscle M-line assembly protein unc-89-like
GFTU01001628.1	38.2±2.2	26.7±0.8	+0.582	3E-13	PREDICTED: muscle M-line assembly protein unc-89-like
GFTU01007383.1	33.9±0.0	23.2±3.4	+0.588	2E-08	PREDICTED: titin isoform X2
GFTU01010045.1	28.3±2.7	20.2±1.2	+0.533	5E-08	PREDICTED: titin-like, partial
GFTU01008365.1	28.6±1.1	20.2±2.0	+0.566	2E-12	PREDICTED: ryanodine receptor
GFTU01008363.1	28.3±1.0	20.0±1.9	+0.565	1E-12	PREDICTED: ryanodine receptor
GFTU01002369.1	19.8±1.0	13.3±3.0	+0.547	3E-04	D-beta-hydroxybutyrate dehydrogenase, putative
GFTU01014213.1	1182.4±91.5	871.7±9.5	+0.519	6E-18	PREDICTED: calcium-transporting ATPase sarcoplasmic/endoplasmic reticulum type isoform X3 (SERCA)
GFTU01010911.1	8.2±1.4	5.9±0.6	+0.505	1E-4	PREDICTED: dynein beta chain, ciliary-like
Proteases					
GFTU01004471.1	134.2±14.5	64.3±13.3	+0.972	5E-14	PREDICTED: cathepsin L1
GFTU01003425.1	135.3±7.5	62.6±11.3	+0.871	2E-07	hypothetical protein g.35645 (Peptidase M1 Aminopeptidase N)
GFTU01001733.1	23.5±0.4	12.8±2.2	+0.872	6E-16	hypothetical protein g.22606 (Peptidase M1 Aminopeptidase N family)
GFTU01012473.1	16.5±2.1	9.6±0.8	+0.716	1E-06	PREDICTED: prostatic acid phosphatase-like
GFTU01013458.1	172.1±18.2	92.9±17.8	+0.638	9E-04	hypothetical protein g.31954 (Chitin-binding domain type 2, Peptidase M1 Aminopeptidase N family)
GFTU01002473.1	27.0±0.7	18.3±1.2	+0.593	2E-08	PREDICTED: neprilysin isoform X1 (membrane metallo-endopeptidase)
GFTU01016619.1	59.8±2.1	42.2±3.8	+0.563	2E-10	PREDICTED: leucyl-cystinyl aminopeptidase-like
GFTU01003281.1	76.7±4.9	54.7±3.4	+0.553	2E-12	PREDICTED: membrane metallo-endopeptidase-like 1 isoform X3
GFTU01012719.1	44.2±2.6	32.5±0.8	+0.515	2E-11	hypothetical protein g.32075 (invasion associated secreted endopeptidase; Provisional)
Extracellular matrix					
GFTU01000571.1	6.3±0.3	3.7±0.1	+0.793	2E-16	PREDICTED: neurogenic locus notch homolog protein 3-like, partial
GFTU01005879.1	28.4±1.7	18.2±0.5	+0.686	5E-14	PREDICTED: neurogenic locus notch homolog protein 1
GFTU01007832.1	24.3±2.2	15.7±2.3	+0.658	1E-9	PREDICTED: membrane-associated guanylate kinase, WW and PDZ domain-containing protein 3-like
GFTU01007834.1	23.9±2.2	15.4±2.5	+0.657	3E-09	PREDICTED: membrane-associated guanylate kinase, WW and PDZ domain-containing protein 3-like
GFTU01007833.1	25.1±2.4	16.2±2.0	+0.655	9E-10	PREDICTED: membrane-associated guanylate kinase, WW and PDZ domain-containing protein 3-like
GFTU01007831.1	25.5±2.4	16.5±1.7	+0.655	3E-10	PREDICTED: membrane-associated guanylate kinase, WW and PDZ domain-containing protein 3-like
GFTU01011451.1	8.3±0.5	5.1±0.0	+0.709	4E-11	hypothetical protein g.48125 (Calcium-binding EGF-like domain)
GFTU01001449.1	7.1±0.2	4.8±0.0	+0.622	1E-13	PREDICTED: uncharacterized protein LOC658528 (Calcium-binding EGF-like domain)
GFTU01001450.1	6.6±0.7	4.5±0.1	+0.583	2E-06	PREDICTED: uncharacterized protein LOC106669909 (Calcium-binding EGF-like domain)
GFTU01001448.1	6.4±0.2	4.6±0.1	+0.540	4E-09	PREDICTED: uncharacterized protein LOC658528 (Calcium-binding EGF-like domain)
GFTU01011448.1	5.4±0.5	3.7±0.4	+0.509	1E-03	PREDICTED: uncharacterized protein LOC106669909 (Calcium-binding EGF-like domain)
GFTU01009271.1	32.3±0.6	23.1±0.6	+0.560	6E-17	PREDICTED: basement membrane-specific heparan sulfate proteoglycan core protein isoform X19
GFTU01009275.1	30.4±0.6	21.9±0.6	+0.551	2E-16	PREDICTED: basement membrane-specific heparan sulfate proteoglycan core protein isoform X7
GFTU01001084.1	31.0±0.6	22.4±0.6	+0.549	3E-16	PREDICTED: basement membrane-specific heparan sulfate proteoglycan core protein isoform X8
GFTU01009272.1	31.2±0.4	22.8±0.5	+0.532	7E-16	PREDICTED: basement membrane-specific heparan sulfate proteoglycan core protein isoform X6
GFTU01009276.1	30.1±0.5	22.0±0.5	+0.531	7E-16	PREDICTED: basement membrane-specific heparan sulfate proteoglycan core protein isoform X13
GFTU01009270.1	30.3±0.4	22.2±0.5	+0.529	9E-16	PREDICTED: basement membrane-specific heparan sulfate proteoglycan core protein isoform X21
GFTU01009274.1	30.2±0.4	22.1±0.5	+0.528	1E-15	PREDICTED: basement membrane-specific heparan sulfate proteoglycan core protein isoform X15
GFTU01009267.1	30.7±0.4	22.5±0.5	+0.526	2E-15	PREDICTED: basement membrane-specific heparan sulfate proteoglycan core protein
GFTU01003839.1	31.1±2.1	22.2±0.6	+0.543	5E-09	PREDICTED: protein mesh isoform X2
Nucleic acid binding					
GFTU01010183.1	10.0±0.1	5.2±0.0	+0.905	1E-14	PREDICTED: piggyBac transposable element-derived protein 4-like
GFTU01001044.1	19.5±2.3	11.8±2.5	+0.532	8E-03	PREDICTED: RNA-directed DNA polymerase from mobile element jockey-like
GFTU01010403.1	11.5±0.1	7.6±0.6	+0.592	4E-06	PREDICTED: retrovirus-related Pol polyprotein from transposon 17.6
GFTU01004281.1	5.7±0.3	3.8±0.9	+0.554	4E-04	PREDICTED: uncharacterized protein K02A2.6-like (2 integrases)
GFTU01004309.1	39.6±1.7	28.3±4.9	+0.522	6E-06	Hypothetical protein g.15643 (integrase)
GFTU01007993.1	11.2±1.1	7.8±0.6	+0.521	2E-04	PREDICTED: nuclear factor interleukin-3-regulated protein

Detoxification					
GFTU01009741.1	23.5±0.6	13.8±0.3	+0.784	2E-14	PREDICTED: venom carboxylesterase-6
GFTU01002688.1	17.8±5.7	6.4±1.4	+0.691	5E-04	PREDICTED: cytochrome P450 4C1-like
GFTU01002689.1	13.1±4.6	4.9±1.2	+0.593	3E-03	PREDICTED: cytochrome P450 4C1-like
GFTU01000057.1	7.8±0.4	5.1±0.4	+0.605	1E-05	PREDICTED: gamma-aminobutyric acid receptor subunit alpha-6-like

***** Contig accessions correspond to BioProject PRJNA393620.

Table 2. Overview of *Euscelidius variegatus* transcripts down-regulated during chrysanthemum yellows (CYp) infection, compared with insects infected by Flavescence dorée (FDp) phytoplasmas. Transcripts were classified into functional categories according to the putative identification assigned by a blastx search.

Contig accession*	FPKM (Average±SD)		Ln Fold change	P value	Sequence description
	Eva_CY	Eva_FD			
Immune response					
GFTU01001177.1	34.4±7.3	70.6±2.9	-0.719	7E-06	PREDICTED: mitogen-activated protein kinase kinase kinase 12 isoform X2
GFTU01016523.1	40.5±6.2	70.1±1.9	-0.654	2E-14	PREDICTED: serine protease snake-like isoform X2
GFTU01005213.1	16.7±4.3	30.7±0.4	-0.635	2E-05	hypothetical protein g.9121 (Kazal-type 1 serine protease inhibitor-like protein type gamma)
GFTU01006779.1	195.0±11.6	307.4±5.2	-0.536	3E-14	hypothetical protein g.7830 (Kazal-type 1 serine protease inhibitor-like protein type gamma)
GFTU01007903.1	6.5±0.3	11.3±0.3	-0.587	4E-05	PREDICTED: protein farnesyltransferase/geranylgeranyltransferase type-1 subunit alpha
GFTU01003663.1	8.0±0.1	13.2±1.2	-0.558	3E-06	PREDICTED: Kruppel-like factor 10
GFTU01003662.1	5.7±0.1	9.4±0.9	-0.534	2E-05	PREDICTED: Kruppel-like factor 10
GFTU01005275.1	16.7±2.1	27.4±0.2	-0.529	1E-04	PREDICTED: circadian clock-controlled protein-like
GFTU01002709.1	11.6±0.9	18.5±1.4	-0.519	4E-06	PREDICTED: heat shock protein 68-like
GFTU01007012.1	8.2±2.1	14.0±2.3	-0.512	4E-34	PREDICTED: pancreatic triacylglycerol lipase-like
Movement and energy metabolism					
GFTU01009515.1	4.7±0.0	8.3±0.0	-0.620	1E-06	dihydropyridine-sensitive l-type calcium channel (DHPR)
Proteases					
GFTU01013038.1	16.0±3.0	27.5±2.4	-0.571	3E-05	PREDICTED: cathepsin D-like
Detoxification					
GFTU01002121.1	15.0±1.2	24.2±0.7	-0.541	4E-07	PREDICTED: probable cytochrome P4506a14

***** Contig accessions correspond to BioProject PRJNA393620.

730 **FIGURE LEGENDS**

731 **FIG 1** Regulation of prophenoloxidase cascade and muscle contraction pathway. During
732 *Euscelidius variegatus* infection with Flavescence dorée (FDp) or Chrysanthemum yellows (CYp)
733 phytoplasmas, prophenoloxidase cascade, which produces melanine as innate immunity response, is
734 oppositely regulated, being activated in FDp and inhibited in CYp-infected insects (**A**). The
735 expression of most of genes involved in muscle contraction was altered upon CYp infection
736 (indicated in colored boxes) (**B**). Scheme was modified from KEGG map 04260: DHPR,
737 dihydropyridine receptor; RyR2, ryanodine receptor; TnC, troponin C; SERCA2a, calcium-
738 transporting ATPase sarcoplasmic/endoplasmic reticulum.
739 Heatmap of expression is indicated: red and green correspond to up- and down-regulation level,
740 respectively, during CYp infection compared with infection by FDp.
741
742 **FIG 2** Phytoplasma infection modulates insect immune response. Gene expression profile indicated
743 as mean normalized relative quantities ± standard error of phenoloxidase (**A**) and Kazal-type 1
744 serine protease inhibitor (**B**) in healthy (H) *Euscelidius variegatus* insects or infected by
745 chrysanthemum yellows (CYp) or Flavescence dorée (FDp) phytoplasmas. Mean enzymatic
746 activities (U) ± standard error of prophenoloxidase (ProPO) measured in plasma (**C**) and haemocyte
747 lysate (**D**) fractions of H, CY, FD insects. (**E**): Box plot of grey intensity calculated for body (dorsal
748 side) of H, CY, FD insects. Grey intensity ranges from 0 (black) to 255 (white). Within the same
749 category (H, CY, FD), asterisks indicate significant differences between female and male of each
750 category. Within the same gender, different letters indicate significant differences among the
751 categories (capitalized for females and small for males). Whenever no sex-related differences were
752 recorded within the same category, female and male data were pooled. (**F**): Mean melanization
753 index (MI, bars) and mean number of adherent cells (dots) (± standard error) measured on nylon
754 threads implanted into H, CY, FD insects. MI ranges from 0 (black) to 1 (white). Different letters

indicate significant differences among the categories (small for MI and capitalized for adherent cells).

FIG 3 Chrysanthemum yellows phytoplasma infection increases energy metabolism. Gene expression profile indicated as mean normalized relative quantities ± standard error of myosin light chain (**A**), tropomyosin (**B**), arginine kinase (**C**) and maltase (**D**) in healthy (H) *Euscelidius variegatus* insects or infected by chrysanthemum yellows (CYp) or by Flavescence dorée (FDp) phytoplasmas. Mean time (seconds) required to leave the 1st circle (bars, Time spent in 1st circle) and mean CO_2 production (dots, Respiration) ± standard error measured in H, CY, FD insects (**E**). Concentric circles used for movement assay (**F**) and leaf mini chamber used for respiration assay (**G** and **H**). Western blot with anti-tropomyosin antisera (**I**) and SDS-PAGE for internal loading control (**L**) of total proteins extracted from H, CY, FD insects. Within the same category (H, CY, FD), asterisks indicate significant differences between female and male of each category. Within the same gender, different letters indicate significant differences among the categories (capitalized for females and small for males). Whenever no sex-related differences were recorded within the same category, female and male data were pooled.

FIG 4 Phytoplasma infection alters protease regulation. Gene expression profile indicated as mean normalized relative quantities ± standard error of cathepsin L isoforms 92i3 (**A**), 92i4 (**B**), 92i6 (**C**) and 473 (**D**) in healthy (H) *Euscelidius variegatus* insects or infected by chrysanthemum yellows (CYp) or by Flavescence dorée (FDp) phytoplasmas. Within the same category (H, CY, FD), asterisks indicate significant differences between female and male of each category. Within the same gender, different letters indicate significant differences among the categories (capitalized for females and small for males). Whenever no sex-related differences were recorded within the same category, female and male data were pooled. Alignment of predicted amino acid sequences for cathepsin L isoforms (**E**): position of signal peptide (grey highlighting), cathepsin propeptide

inhibitor domain (I29) and mature protease domains are indicated above the alignment; predicted glycosylation sites are indicated as single boxed amino acid (white: N-glycosilation; grey: O-glycosilation); highly conserved regions containing the three cathepsin L-typical consensus sequences are boxed, bold and required conserved amino acids within each consensus sequence are located above the sequences; immunogenic peptide sequence is boxed and aligned below the sequences; three predicted active sites are indicated by black full arrowheads; predicted isoelectric point and molecular weight of pre-proteins and mature forms are indicated at the end of each sequence. Percent identity matrix of the four cathepsin L isoforms and immunogenic peptide (**F**): values for pre-proteins are indicated bottom left of the matrix, mature forms in italics up right of the matrix. Western blot with anti-cathepsin L antisera (**G**) and SDS-PAGE for internal loading control (**H**) of total proteins extracted from H, CY, FD insects.

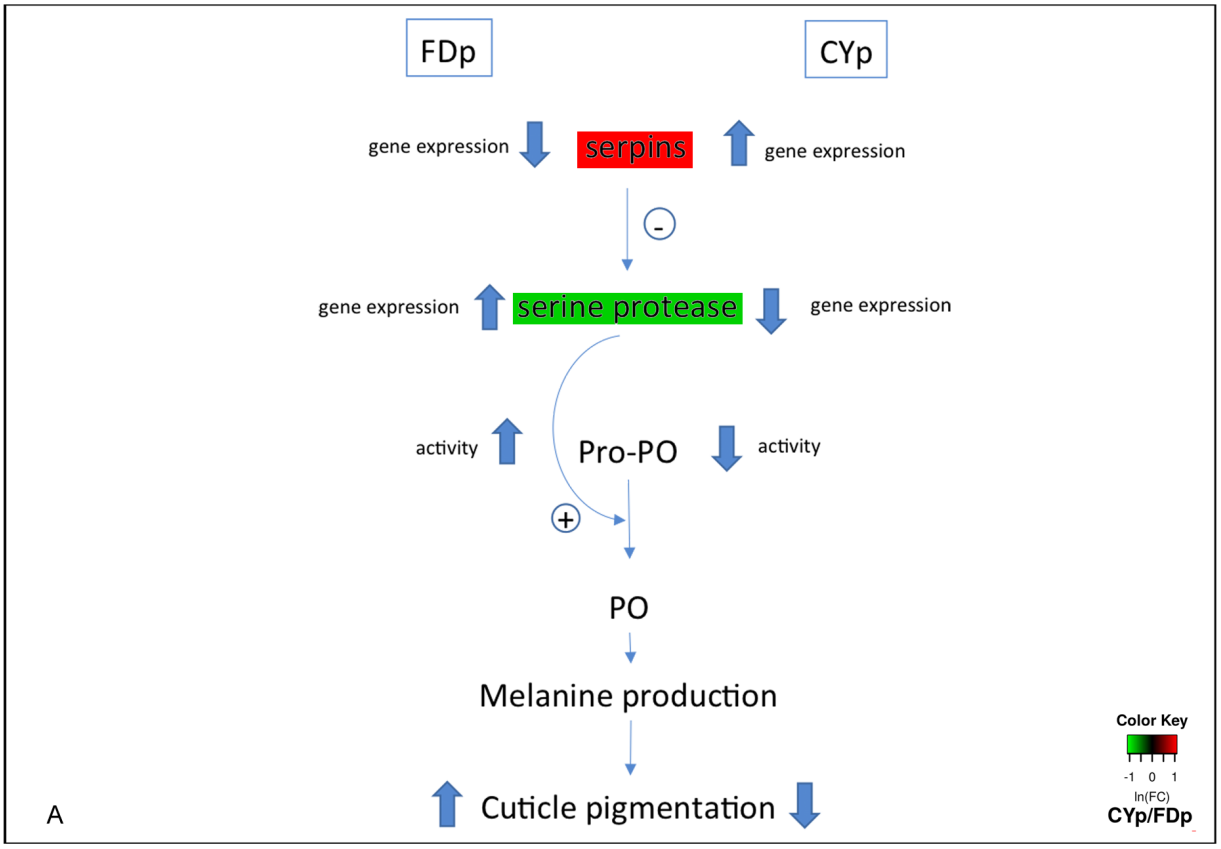

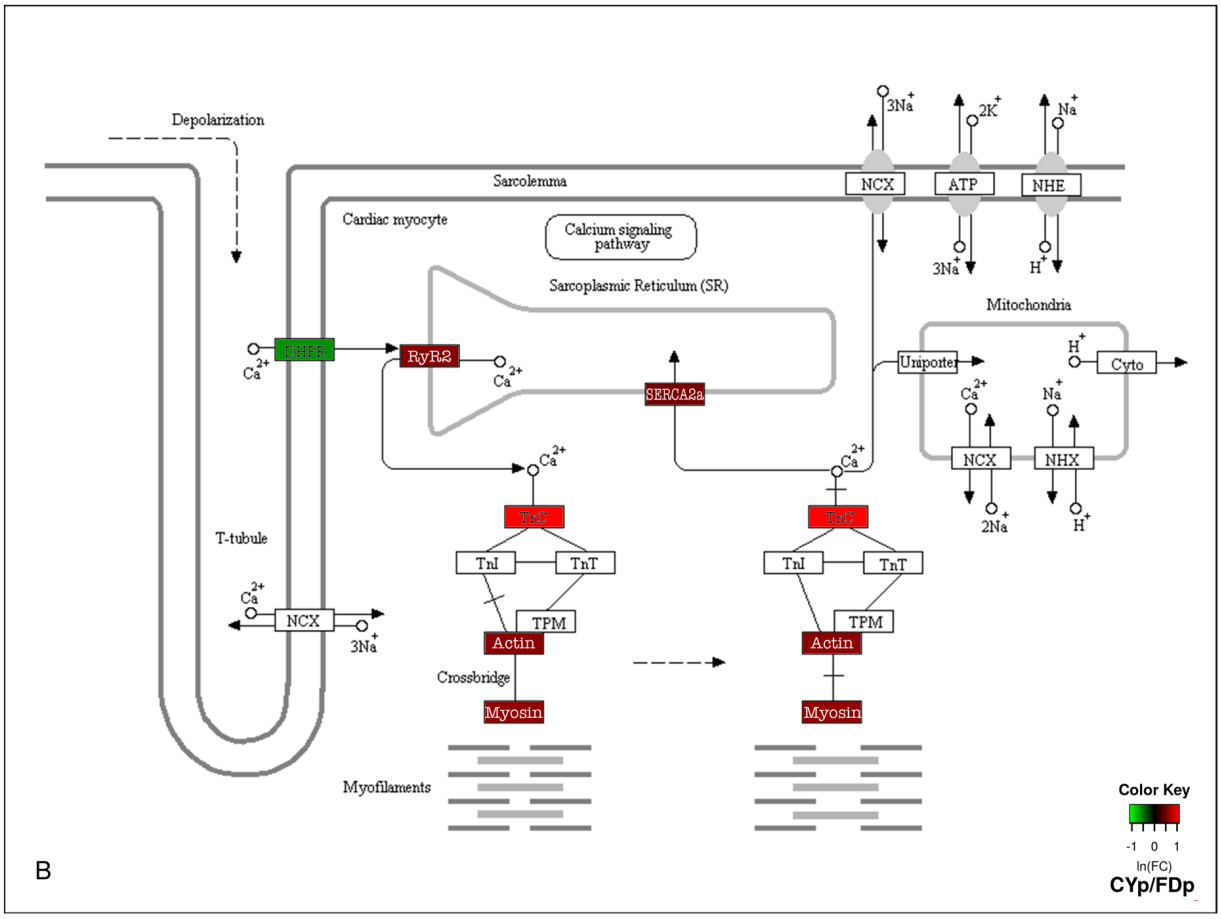

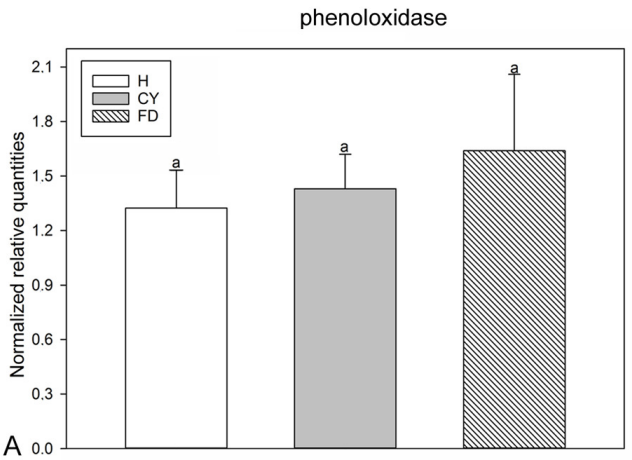

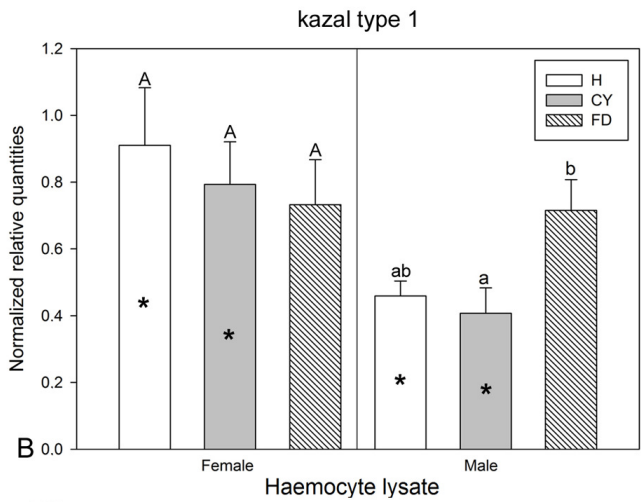

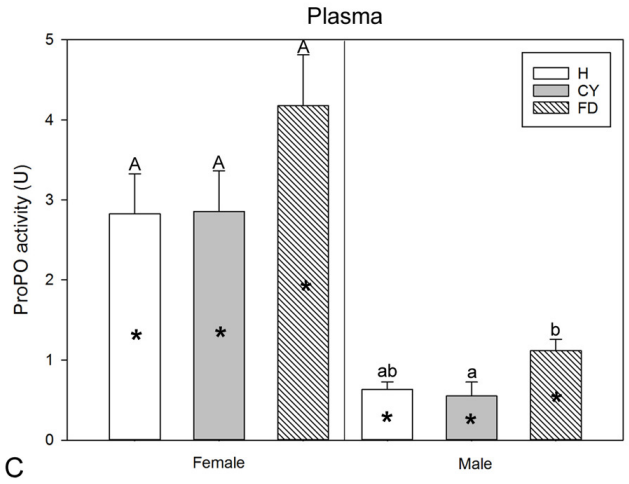

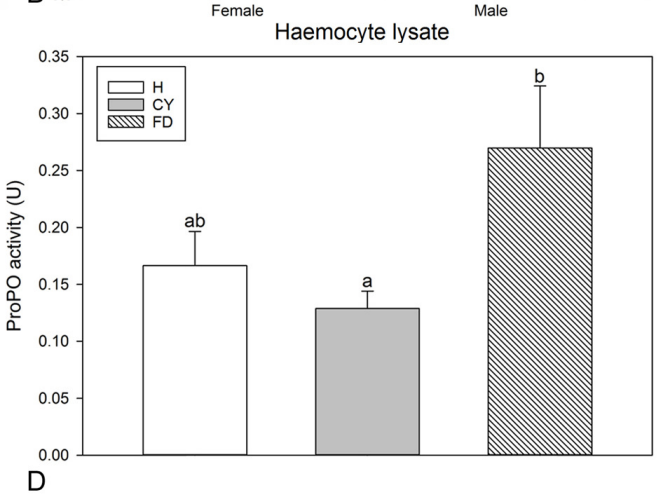

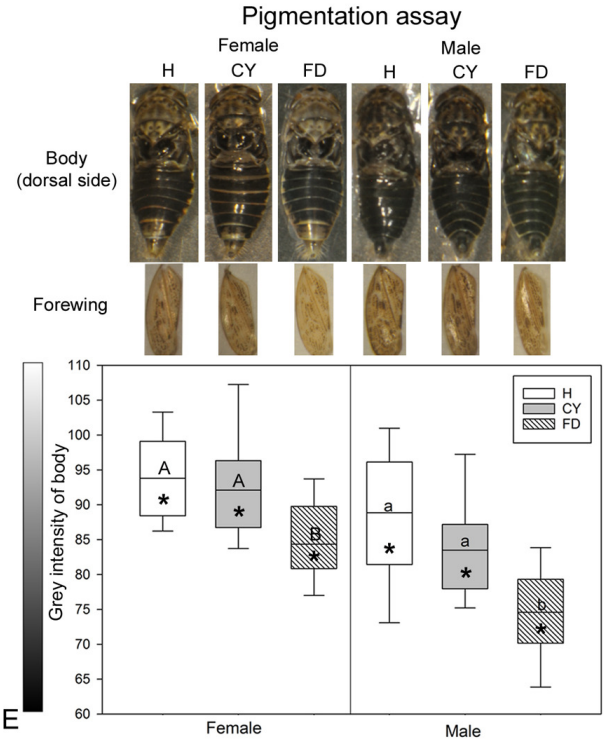

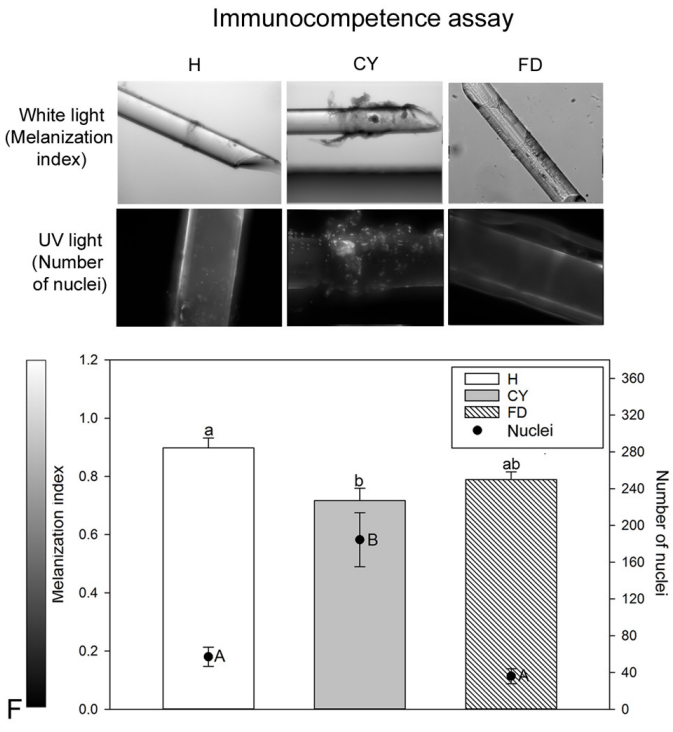

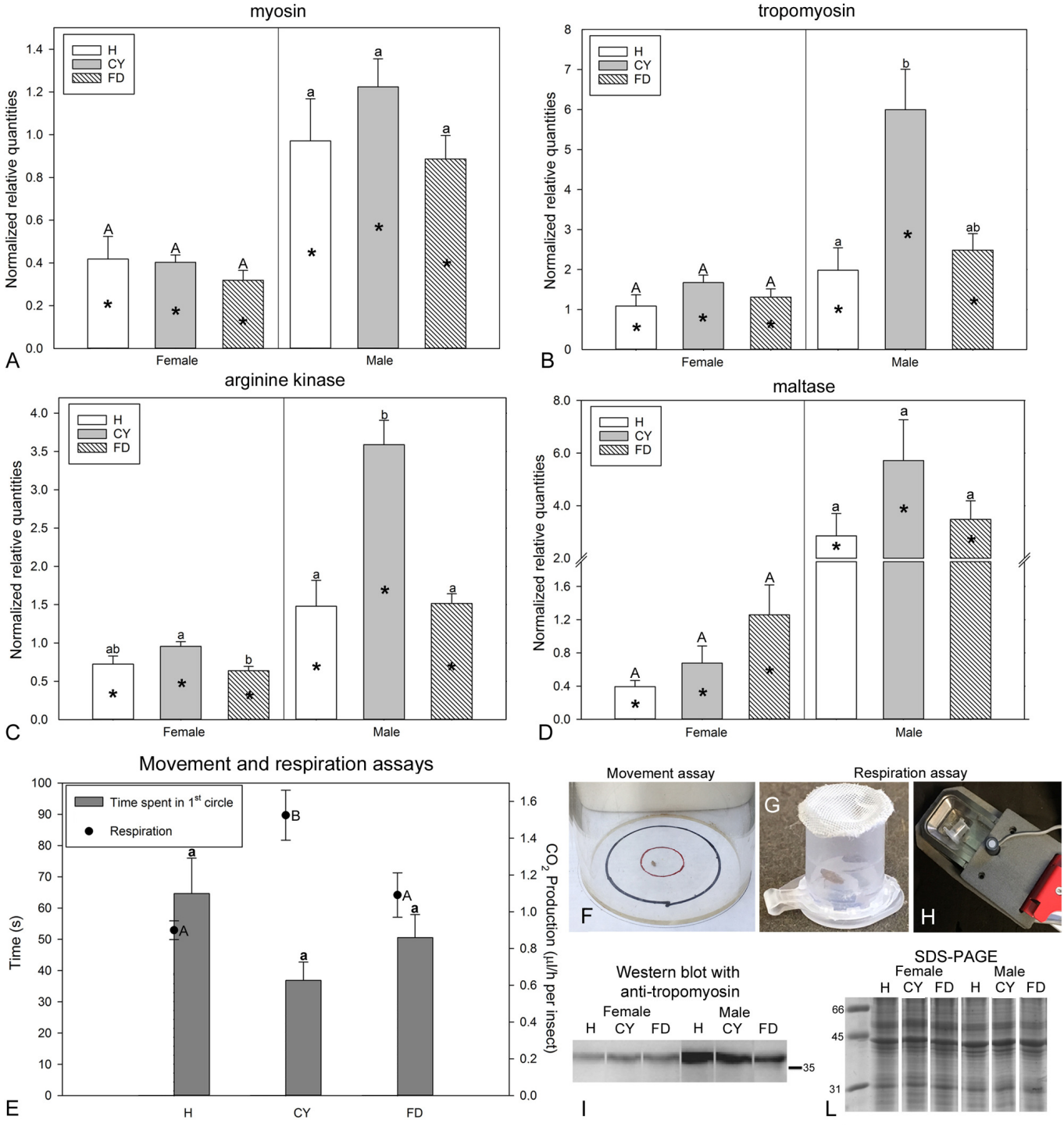

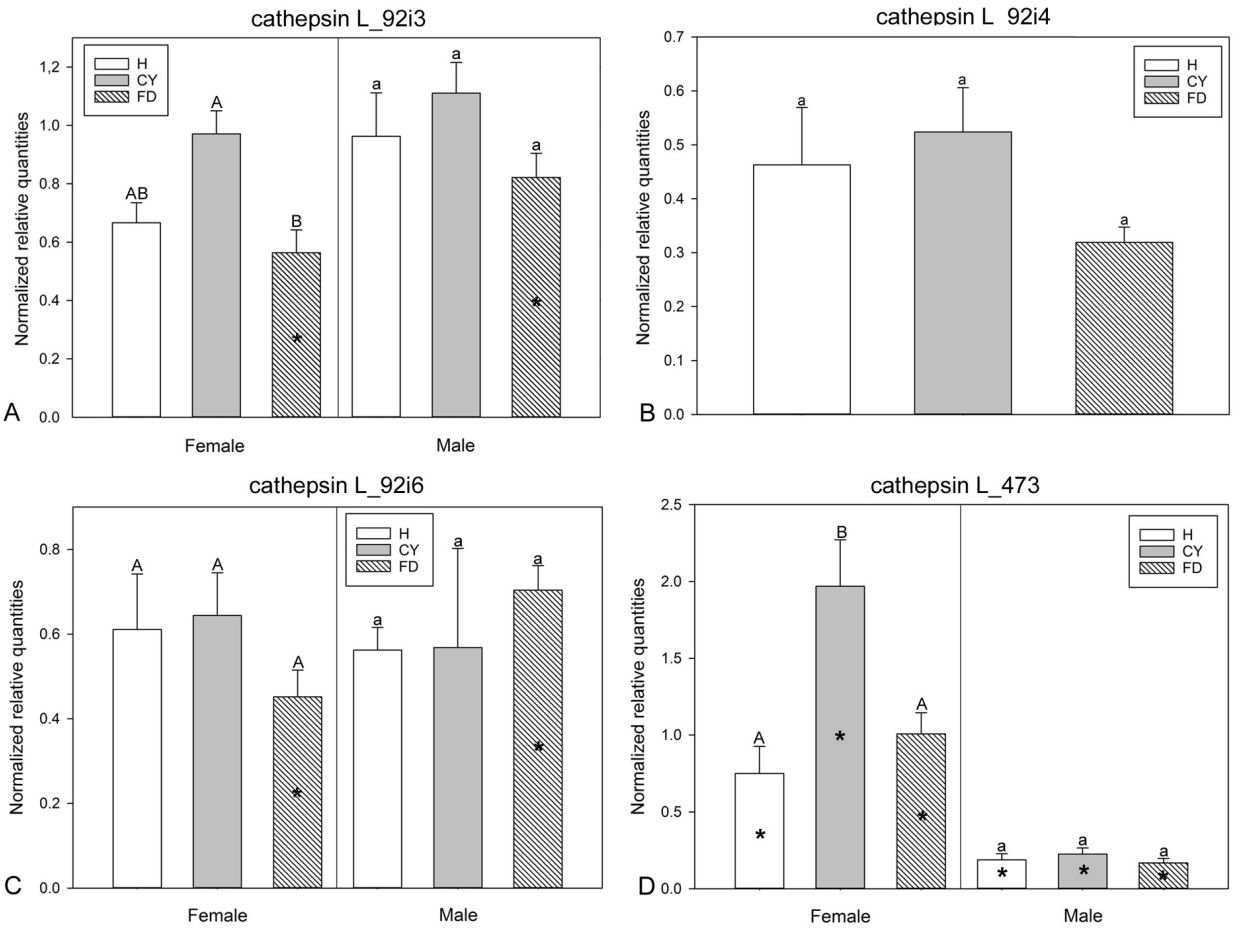

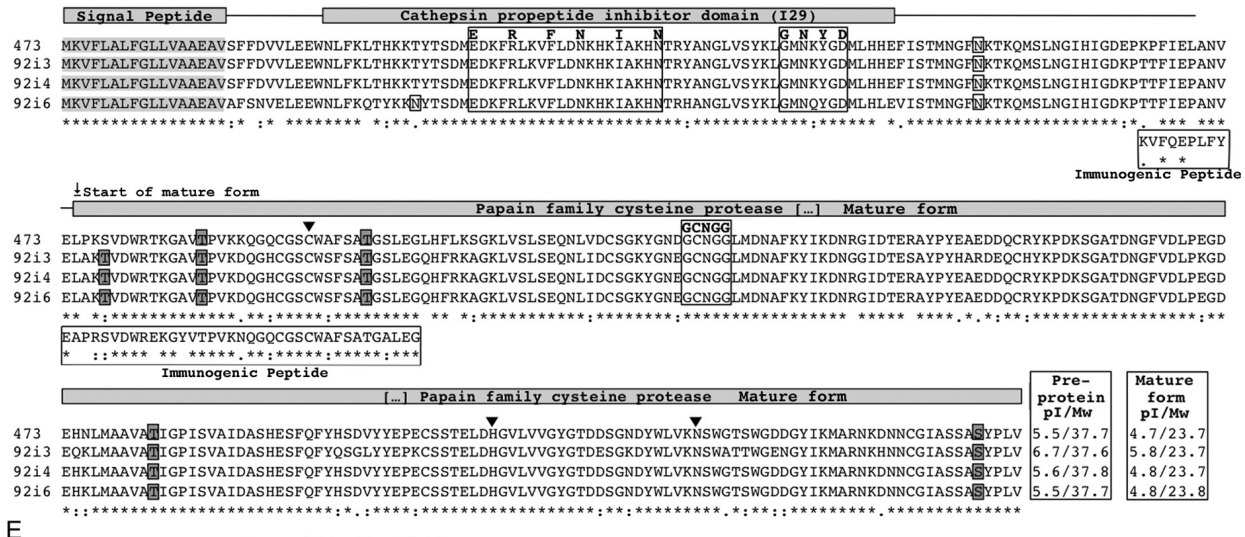

E

Percent Identity Matrix

F

	Alignment on pre-protein				Alignment on mature form
	473	92i3	92i4	92i6	Immunogenic Peptide
473	/	86.24	94.95	94.95	83.33
92i3	89.97	/	91.28	91.28	72.22
92i4	95.58	94.40	/	100.00	72.22
92i6	92.33	91.15	96.76	/	72.22
Immunogenic Peptide	73.91	65.22	65.22	65.22	/

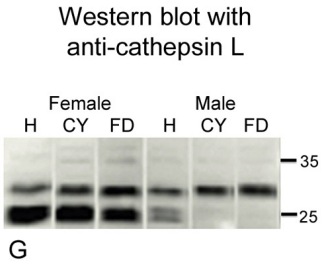

G

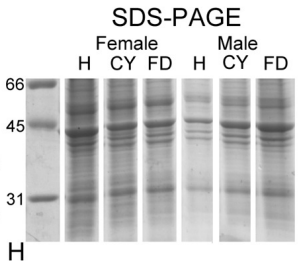

H